Research

New Phytologist

Meiotic pairing irregularity and homoeologous chromosome compensation cause rapid karyotype variation in synthetic allotetraploid wheat

Jing Zhao[1]*, Juzuo Li[1]*, Ruili Lv[1], Bin Wang[1], Zhibin Zhang[1], Tingting Yu[1], Shuhan Liu[1], Hongwei Xun[1], Chunming Xu[1], Jonathan F. Wendel[2] and Bao Liu[1]

[1]Key Laboratory of Molecular Epigenetics of the Ministry of Education (MOE), Northeast Normal University, Changchun 130024, China; [2]Department of Ecology, Evolution & Organismal Biology, Iowa State University, Ames, IA 50011, USA

Authors for correspondence:
Chunming Xu
Email: xucm848@nenu.edu.cn

Bao Liu
Email: baoliu@nenu.edu.cn

Received: *22 December 2022*
Accepted: *5 April 2023*

New Phytologist (2023) **239:** 606–623
doi: 10.1111/nph.18953

Key words: allopolyploidization, karyotypic diversification, meiotic instability, phenotypic variation, synteny, synthetic allopolyploid.

Summary

- Allopolyploidization may initiate rapid evolution due to heritable karyotypic changes. The types and extents of these changes, the underlying causes, and their effects on phenotype remain to be fully understood.
- Here, we designed experimental populations suitable to address these issues using a synthetic allotetraploid wheat.
- We show that extensive variation in both chromosome number (NCV) and structure (SCV) accumulated in a selfed population of a synthetic allotetraploid wheat (genome S^bS^bDD). The combination of NCVs and SCVs generated massive organismal karyotypic heterogeneity. NCVs and SCVs were intrinsically correlated and highly variable across the seven sets of homoeologous chromosomes. Both NCVs and SCVs stemmed from meiotic pairing irregularity (presumably homoeologous pairing) but were also constrained by homoeologous chromosome compensation. We further show that homoeologous meiotic pairing was positively correlated with sequence synteny at the subtelomeric regions of both chromosome arms, but not with genic nucleotide similarity *per se*. Both NCVs and SCVs impacted phenotypic traits but only NCVs caused significant reduction in reproductive fitness.
- Our results implicate factors influencing meiotic homoeologous chromosome pairing and reveal the type and extent of karyotypic variation and its immediate phenotypic manifestation in synthetic allotetraploid wheat. This has relevance for our understanding of allopolyploid evolution.

Introduction

Allopolyploidy, by coupling interspecific hybridization and whole genome duplication (WGD), has been widely documented as an important force driving speciation and evolution of angiosperms (Wendel, 2000; Jiao *et al.*, 2011; Soltis *et al.*, 2015; Van de Peer *et al.*, 2017). One source of genetic variation associated with allopolyploidy is rapid genomic changes immediately following allopolyploidization due to perturbation of meiosis and incompatible genetic interactions between the abruptly merged genomes (Adams & Wendel, 2005; Otto, 2007; Doyle *et al.*, 2008; Gonzalo, 2022; Shimizu, 2022). In contrast to a slower process of stepwise accumulation of random mutation followed by natural selection, allopolyploidization-induced rapid genomic changes can be saltational and enable rapid diversification (Wendel, 2000; Comai, 2005; Otto, 2007; Soltis & Soltis, 2009; Van de Peer *et al.*, 2021). The types and extents of such genomic changes immediately following allopolyploidization have begun to be clarified in some systems (Comai, 2005; Gaeta & Chris Pires, 2010; Xiong *et al.*, 2011; Chester *et al.*, 2012; Mandáková & Lysak, 2018; Mandáková *et al.*, 2019; Mason & Wendel, 2020; Ferreira de Carvalho *et al.*, 2021).

Common wheat (*Tritium aestivum* L.) is a staple food crop of global importance, and a textbook example of speciation via allopolyploidization (Feldman & Levy, 2012). Formation of bread wheat involves two allopolyploidization events: allotetraploidization between the B-subgenome progenitor species (BB) and *Tritium urartu* (AA) led to formation of allotetraploid wheat *Tritium turgidum* (BBAA) *c.* 0.8 million years ago (Marcussen *et al.*, 2014), and then allohexaploidization between a domesticated form (e.g. subsp. *dicoccum* or *durum*) of *T. turgidum* (BBAA) and *Aegilops tauschii* (DD) enabled speciation of *T. aestivum* (BBAADD) *c.* 8500 yr ago (Levy & Feldman, 2022).

Tritium turgidum and *A. tauschii* can be artificially hybridized to generate synthetic allohexaploid wheats, which have been widely used to study the immediate effects and consequences of

*These authors contributed equally to this work.

allohexaploidization (Feldman *et al.*, 2012). The types (genetic, gene expression, and epigenetic) and extents of changes associated with allohexaploidization in wheat have been widely studied (Ozkan *et al.*, 2001; Shaked *et al.*, 2001; Mestiri *et al.*, 2010; Kenan-Eichler *et al.*, 2011; Zhao *et al.*, 2011; Jighly *et al.*, 2019), with a common finding being that rapid genomic changes at the molecular level follow polyploidy (Jighly *et al.*, 2019; Levy & Feldman, 2022). At the chromosomal level, numerical variation, that is, whole-chromosome aneuploidy, also is common, but structural karyotypic variation is uncommon in synthetic allohexaploid wheat (Zhang *et al.*, 2013b), probably due to presence of the homoeologous pairing control genes like *Ph1* and *Ph2* (Sears, 1976; Griffiths *et al.*, 2006; Martín *et al.*, 2021; Serra *et al.*, 2021) inherited from the maternal parent, *T. turgidum*. At the tetraploid level, because the B-subgenome donor species is not available, a synthetic allotetraploid wheat with the same genome constitution as *T. turgidum* cannot be obtained, but various allotetraploid wheats have been constructed using different combinations of diploid *Aegilops* and *Triticum* species (Ozkan *et al.*, 2001). Studies using these synthetic allotetraploids have indicated more extensive and rapid genomic changes at the molecular level (Ozkan *et al.*, 2001; Kashkush *et al.*, 2002) than those found in synthetic allohexaploid wheat. In particular, dramatic karyotypic variation, including changes in both chromosome number and structure, were observed (Zhang *et al.*, 2013a; Gou *et al.*, 2018; Lv *et al.*, 2022), indicating lack of a genetic pairing control system in the diploid parental species. Using synthetic allotetraploids AADD, derived from *T. urartu* (AA) and *A. tauschii* (DD) (Gou *et al.*, 2018), and S^lS^lAA, derived from *Aegilops longissima* (S^lS^l) and *T. urartu* (AA) (Lv *et al.*, 2022), we investigated the meiotic pairing behavior of homoeologous chromosomes, the types of karyotypic variants that were precipitated after successive sexual propagation (via selfing), as well as the effects of chromosomal variation on phenotypes in these two synthetic allotetraploid wheats. Notably, similar to findings in other allopolyploid plants (Nicolas *et al.*, 2009; Leal-Bertioli *et al.*, 2015; Chen *et al.*, 2018; Ferreira de Carvalho *et al.*, 2021), an intriguing observation emerged from these prior studies is the substantial differences between subgenomes and chromosomes in both meiotic pairing behavior and the chromosomal consequences thereof. However, factors underlying these *cis*-acting differences are yet to be explored. In addition, although all organismal karyotypic variants likely originated from meiotic chromosome pairing irregularity, whether there are other factors, such as differential homoeologous compensation, which might also contribute to the spectrum of variable NCVs and SCVs remains unknown.

To further understand the pattern and process underlying rapid karyotypic evolution in synthetic allopolyploid wheat, we designed experiments using a newly constructed synthetic allotetraploid wheat (S^bS^bDD) between *Aegilops bicornis* (S^bS^b, ♀) and *A. tauschii* (DD, ♂). These two *Aegilops* species have diverged substantially from each other during *c.* 5 million years of separation, including differential introgressions (Marcussen *et al.*, 2014; Ruban & Badaeva, 2018; Glémin *et al.*, 2019; Li *et al.*, 2022). Specifically, we constructed two experimental populations using this synthetic allotetraploid wheat: one was a 'genetic variant-accumulation population' propagated from a single, euploid founder for eight successive selfed generations without cytogenetic selection during the intervening generations, and the other was a 'multigenerational euploidy-selecting population' starting from an euploid plant from the same first generation (S1) euploid founder individual whereby only euploid plants were selected to produce the next generation (Supporting Information Figs S1, S2). Based on parallel characterization of the two populations, we document extensive karyotypic variants that accumulated in the populations, which stemmed from meiotic instability (presumably homoeologous pairing) and which often contained interhomoeologues compensation. We also demonstrate that the degree of homoeologous pairing was positively correlated with interhomoeologues sequence synteny, but not with genic nucleotide similarity *per se*, and the correlations are significant only at the subtelomeric regions of both chromosome arms. Our results implicate deterministic genetic factors impacting differences in meiotic stability among chromosomes, convey the type and magnitude of organismal karyotypic variation that can result, and reveal impacts on phenotypic variation and reproductive fitness.

Materials and Methods

Plant materials

The synthetic allotetraploid wheat (genome S^bS^bDD, $2n = 28$) was produced by crossing *A. bicornis* (S^bS^b, $2n = 14$, accession TB01, ♀) and *A. tauschii* (DD, $2n = 14$, accession TQ27, ♂), followed by colchicine-mediated chromosome doubling (Fig. S1a). We conducted an initial cytological analysis of a set of seedlings of the first selfed generation (S1) of this synthetic allotetraploid wheat by the sequential use of fluorescence *in situ* hybridization (FISH) and genomic *in situ* hybridization (GISH), which allowed reliable identification of each chromosome of the S^b and D subgenomes (Zhang *et al.*, 2013a). We found this synthetic allotetraploid wheat was unstable in karyotype and manifested chromosomal variation in both number and structure. We thus arbitrarily selected a single S1 euploid plant whose fertility (defined as total seed no./plant) was *c.* 33%, an average of all euploid individuals, and produced the S2 population. We then identified the first two euploid S2 plants also with a fertility of euploidy average (*c.* 32–35%) in the cytogenetic screening, and used these two sibling S2 euploid plants to generate the two populations used in this study. First, we constructed a 'genetic variant-accumulation population' (henceforth termed population I). Specifically, we used one of the two euploid S2 plants to propagate via selfing for six more generations until S8 (Fig. S1b). In the course of this propagation, we first randomly chose six seeds from the bulk (*c.* 80%) of the S3 plants that showed a relatively higher fertility (25–35%; the rest *c.* 20% plants with clearly lower fertility were not chosen), then from S4 to S8, we randomly chose three seeds from each plant (with fertility being in the range of 25–35%) to produce the next generation; in the entire course, we did not impose any trait-based selection (except for representative fertility) or cytological analysis. We obtained 1458 individuals in the S8 population. We karyotyped all 1458 individuals by FISH and GISH and were able to determine karyotypes of 1322 individuals (Table S1). The other S2 euploid individual was used to construct a 'multigenerational euploidy-selecting population' (henceforth

termed population II). Specifically, we propagated this euploid plant via selfing for eight additional generations until S10, conducting FISH/GISH-based cytological analysis at each generation, and only selecting a subset of euploid individuals randomly (all euploid plants showed similar fertilities, 25–35%) to produce the next generation (Fig. S2). We obtained karyotypes for a total of 487 individuals that were the immediate progenies of euploid parents. Also, we randomly chose 10 euploid individuals from S4 and S6 (five from each generation) for meiotic analysis.

Mitotic and meiotic karyotyping by FISH and GISH

Root-tip cells and meiocytes were used for mitotic and meiotic karyotyping, respectively, by sequential FISH and GISH. The sequential FISH and GISH procedures were essentially as reported (Han *et al.*, 2004; Kato *et al.*, 2004) with minor modifications (Zhang *et al.*, 2013a). The detailed procedures are presented in Methods S1 and Notes S1.

Comparative genomic analysis of the two diploid parental species, *A. bicornis* and *A. tauschii*

All published sequencing data and their annotations used in this study were retrieved from the National Center for Biotechnology Information (NCBI), which included *A. tauschii* (genome DD) (Luo *et al.*, 2017) and *A. bicornis* (genome S^bS^b) (Li *et al.*, 2022).

MUMmer v.3.9. pairwise sequence comparisons were performed between each of the seven sets of homoeologous chromosomes of *A. bicornis* and *A. tauschii*. After preliminary mapping by NUCMER (the parameters were set as 'nucmer --mum -c 90 -l 40 -p'), low quality, and short length of the alignment fragments were filtered by delt-filter (the parameters were set as 'delta filter -m -i 95 -l 100'). Then, position and mapping information regarding the alignment data were acquired by show-coords. The Synteny and Rearrangement Identifier (SyRI) programs were used to obtain structural and syntenic blocks between each pair of homoeologous chromosomes from show-coords operated results (Kurtz *et al.*, 2004). Detailed syntenic path identification was formed using a directed acyclic graph approach (Goel *et al.*, 2019). Syntenic blocks were detected by a customized PYTHON script. Percent of sequence identity of genic regions and transposable elements (TEs) ratios were calculated by customized R and PYTHON scripts.

Gene content and TE length distributions were calculated using a sliding window of 10 Mb, with a step of 1 Mb along the entire chromosome length to predict the centromere region on each chromosome of *A. bicornis* and *A. tauschii*, according to previously reported methods (Choulet *et al.*, 2014). Each chromosome arm was divided into a given number (n) of equal-length (in nt) windows along with the centromere region (thus a total of $2n+1$ windows for each chromosome; Fig. S3a). The proportion of syntenic sequence against the total length in each window between *A. bicornis* and *A. tauschii* was calculated. Pearson's correlations between the amount of homoeologous chromosome pairing irregularity at MI and the proportion of syntenic sequence in n^{th} window were tabulated (Fig. S3b).

Phenotyping

Eight morphological traits reflecting growth, development, and reproductive fitness, that is, plant height, tiller number, spike length, spikelet number per spike, grain length, grain width, seed setting/individual, and one hundred-kernel weight, were measured at maturity for all karyotyped individuals of the S8 population of the synthetic allotetraploid wheat. For quantification, individuals were grouped according to their karyotypes.

Statistics

R statistical analysis software (I386 4.0.2) was used for statistical analysis and graphic presentation of all data are presented in Methods S1.

Results

Extensive karyotype variation in selfed progenies

We karyotyped a total of 1322 individuals from an 8^{th} selfed generation (S8) population descended from a single S1 euploid founder plant of a synthetic allotetraploid wheat (genome S^bS^bDD) (Fig. S1). Because no selection was exerted except for an average fertility of the 80% bulk plants during the intervening generations and plants at each generation were randomly chosen among the 80% bulk to produce the next generation, this S8 population constituted the 'genetic variant-accumulation population' (population I). We identified extensive chromosomal variation in both number and structure in this set of plants, which together displayed extensive karyotypic heterogeneity within the population (Table S1). The 1322 individuals could be divided into three major groups based on whether numerical chromosomal variations (NCVs) occurred and the types thereof, which were: (1) euploidy ($2n=28$, $S^b=14/D=14$), (2) compensated aneuploidy, that is, balanced loss and gain of homoeologous chromosomes ($2n=28$, $S^b\neq14/D\neq14$), and (3) noncompensated aneuploidy including hidden aneuploidy, that is, gain and loss of nonhomologous chromosomes that can be either nonbalanced ($2n\neq28$) or balanced ($2n=28$, $S^b=14/D=14$) (Fig. 1a,b). Each of these groups could be further categorized into two subgroups, that is, those that contained structural chromosomal variations (SCVs) and those that did not, thus, giving rise to six distinct plant categories. Among these six categories, only 13.2% (174 of the 1322 karyotyped individuals) are *bona fide* euploids, while the two categories 'euploidy with SCVs' and 'compensated aneuploidy with SCVs' comprised 44.4% (587 of 1322) and 35.2% (465 of 1322) of the total, respectively (Fig. 1a).

In contrast to the *bona fide* euploidy category, which possessed a single common karyotype, the other five categories each contained variable karyotypes. We found that the two categories, euploidy with SCVs and compensated aneuploidy with SCVs, were composed of diverse karyotypes, containing 444 and 375 distinct chromosome compositions, respectively (Fig. 1c). The remaining categories also contained variable karyotypes but to a much lower degree, probably due to limited numbers (Fig. 1c).

(a)

Euploid (S = 14/D = 14) (761)		Compensated aneuploid (S ≠ 14/D ≠ 14) (481)		Non-compensated aneuploid (80)		
No-SCV	SCV	No-SCV	SCV	No-SCV	SCV	Hidden
174	587	16	465	8	71	1
13.16%	44.40%	1.21%	35.17%	0.60%	5. 29%	0.076%

(b)

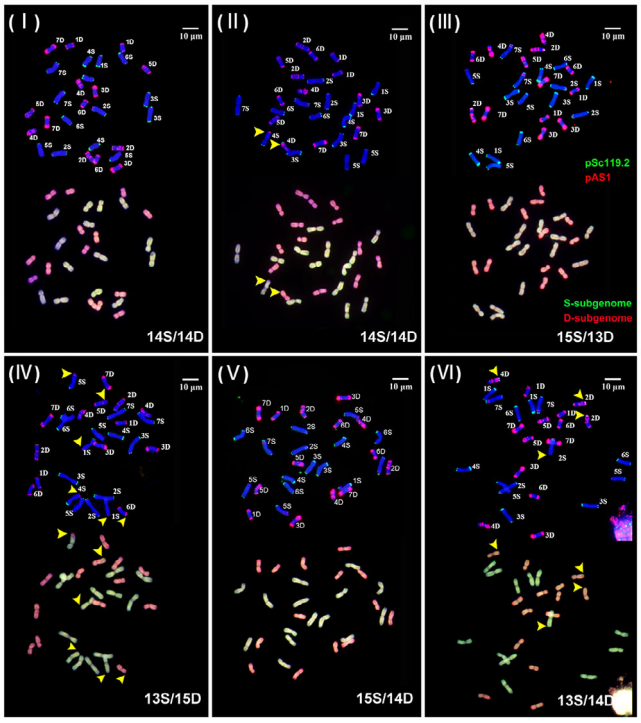

(c)

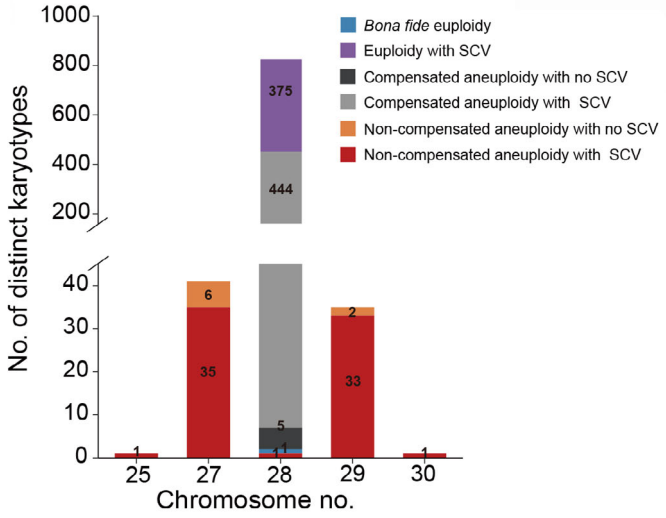

Fig. 1 Variation in chromosome number (NCVs) and structure (SCVs) in 1322 karyotyped individuals at S8 of the 'genetic variant-accumulation population' (population I) of synthetic allotetraploid wheat (S^bS^bDD), categorization of the six karyotype groups, and representative fluorescence *in situ* hybridization (FISH) and genomic *in situ* hybridization (GISH) images. (a) The 1322 individuals could be divided into three major groups according to presence or absence of NCVs; the number and percent of individuals belonging to each group and subgroup are shown. (b) Representative FISH and GISH images of the six subgroups: (I) *bona fide* euploidy; (II) euploidy with SCV; (III) compensated aneuploidy with no SCV; (IV) compensated aneuploidy with SCV; (V) noncompensated aneuploidy with no SCV; and (VI) noncompensated aneuploidy with SCV. The pAs1 (red signals) and pSc119.2 (green signals) tandem repeats were used as FISH probes. Genomic DNAs of *Aegilops bicornis* (S^bS^b, green signals) and *Aegilops tauschii* (DD, red signals) were used as GISH probes. Yellow arrowheads indicate chromosomes containing translocations. (c) The numbers of distinct karyotypes harbored by each of the six karyotype categories.

Thus, the combination of NCVs and SCVs generated a total of 904 distinct karyotypes among the 1322 individuals descended from a single founder euploid plant after only eight generations of selfing. If one assumes that the NCVs and SCVs accumulate evenly across generations, this would give rise to a high rate of karyotypic divergence, > 9% (74%/8) per generation.

Differential frequencies of numerical and structural chromosomal variation among chromosomes and between subgenomes

Of the 1322 karyotyped individuals, 561 showed NCVs, of which 537 (95.7%) contained SCVs, while the other 24 (4.3%) did not. Because the number of the second type was small, we combined both types for NCV analyses. We tabulated the numbers of NCVs for each of the 14 homologous chromosome pairs across these 561 plants, finding substantial differences with respect to their propensities to undergo aneuploidy, that is, whole chromosome(s) loss or gain (Fig. 2a). Given that the majority (85.7%) of these plants (481 of 561) were compensated aneuploids, it was perhaps not surprising that homoeologous chromosome pairs tended to show very similar frequencies of NCVs but with contrasting patterns in terms of loss vs gain of chromosome (s). The group 5 homoeologous chromosomes ($5S^b$ and 5D) showed the highest frequencies of NCVs (Wilcoxon test, all *P*-values < 0.001), which were followed by groups 4, 3, 2, and 1 homoeologous chromosomes in a descending order, while the groups 6 and 7 homoeologous chromosomes showed the smallest number of NCVs (Wilcoxon test, all *P*-values < 0.001) (Fig. 2b). Of note, the S^b-subgenome showed more gain than loss of chromosomes (Wilcoxon test, *P*-value = 0.03461), while the D-subgenome showed the opposite trend (Wilcoxon test, *P*-value = 0.03429) (Fig. 2c,d). These trends were also reflected by distribution of plants across the variable chromosomal complements; in both compensated and noncompensated aneuploid groups, substantially more individuals had more S^b- than D-subgenome chromosomes (Fig. 2c,d). Thus, rapid karyotypic evolution in this system is strongly shaped by subgenome-biased chromosome gain or loss.

Of the 1322 karyotyped individuals, 1148 (86.9%) harbored SCVs (Fig. 1a,c). Of these, 587 (51%) were euploid and 561 (49%) were aneuploid (Fig. 1a,c). We analyzed the trends of SCVs in each group and found they were similar. The SCVs were diverse in both plant groups and occurred in all 14 homologous chromosome pairs of both subgenomes and both arms were involved (Fig. 3). The SCVs primarily reflected the loss of chromosomal segments and/or gain of corresponding segments from the homoeologous chromosomes, with the segments being either

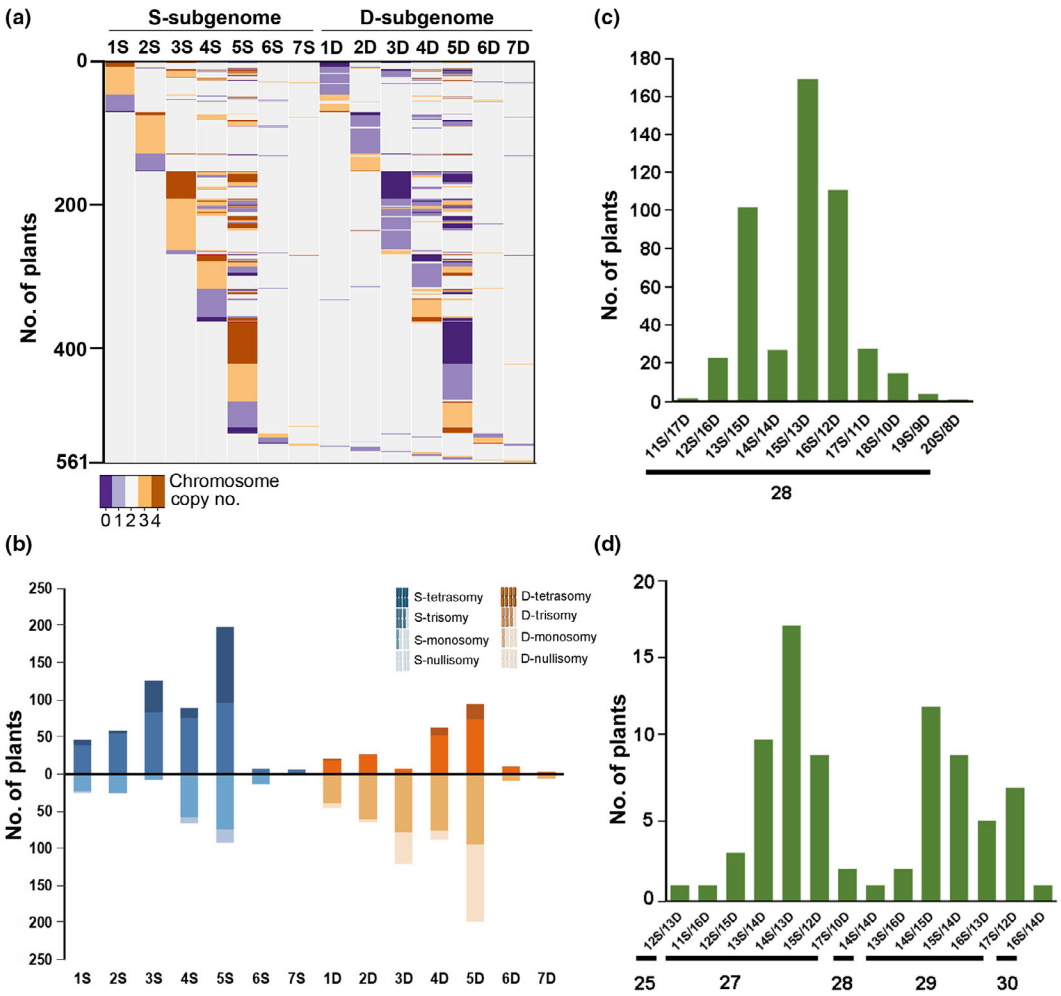

Fig. 2 Differences in frequencies of numerical chromosome variants (NCVs) among chromosomes and between the two subgenomes in population I (at S8) of the synthetic allotetraploid wheat (S^bS^bDD). (a) Heatmap depicting NCVs among the 14 chromosomes of the S^b- and D-subgenomes of 561 individuals that contained NCVs. Color key representing chromosome copy numbers from 0 to 4. (b) Stacked bar chart depicts NCVs manifested by each chromosome. The *x*-axis denotes the 14 chromosomes of the S^b- and D-subgenomes. Above and below the *x*-axis are shown gain and loss of either one homolog (lighter colors) or both homologs (darker colors), respectively. The *y*-axis represents the number of individuals with NCVs. (c) Different types of compensated aneuploidy ($2n = 28$). The *x*-axis represents the different NCV types of compensated aneuploidies that all had a chromosome number of $2n = 28$; *y*-axis represents the number of plants. (d) Different types of noncompensated aneuploidies ($2n \neq 28$). The *x*-axis represents different NCV types, the numbers below the black line represent the chromosome numbers ($2n = 25$, 27, 28, 29, and 30, respectively), *y*-axis represents the number of plants. Note that here the $2n = 28$ aneuploidies were still noncompensated as they did not show equal NCVs of homoeologous chromosomes.

terminal or intercalary, and of variable sizes (Fig. 3). No Robertsonian translocations were detected, suggesting no functional deterioration of centromeres. Both the quantity and variety of SCVs differed dramatically among the 14 homologous chromosome pairs in both plant groups (Figs 3, 4a). Notably, the two pairs of homoeologous chromosomes for a given group showed largely similar proportions of SCVs (Fig. 4b), suggesting that the SCVs mainly originated from meiotic homoeologous exchanges (HEs), as detailed in later sections. In spite of the among-chromosome differences, when each subgenome was considered as a whole, there were no significant differences in the numbers of SCVs between the two subgenomes in both plant groups (Wilcoxon test, *P*-values = 0.8957 and 0.4508, respectively), in contrast to the NCVs discussed above.

Although the euploid and aneuploid plant groups showed similar trends in SCVs (Fig. 4a), both the quantity and distribution of SCVs were significantly different between the two groups. The aneuploid plant group showed both more (Wilcoxon paired test, *P*-value = 0.03125) and broader distribution (chi-squared test, *P*-value = 2.2E-16) of SCVs than did the euploid plant group (Fig. 4c,d), indicating that SCVs were positively correlated with NCVs, probably because either aneuploidy had a higher buffering capacity than euploidy to sustain SCVs, or perhaps because the two kinds of chromosomal variation were functionally compensating or constraining each other (Schubert & Lysak, 2011), as detailed in the following section.

Variable homoeologous compensation among the seven chromosome groups

The concordance between homoeologous chromosome pairs in their representation in both NCVs and SCVs (Figs 2–4) may

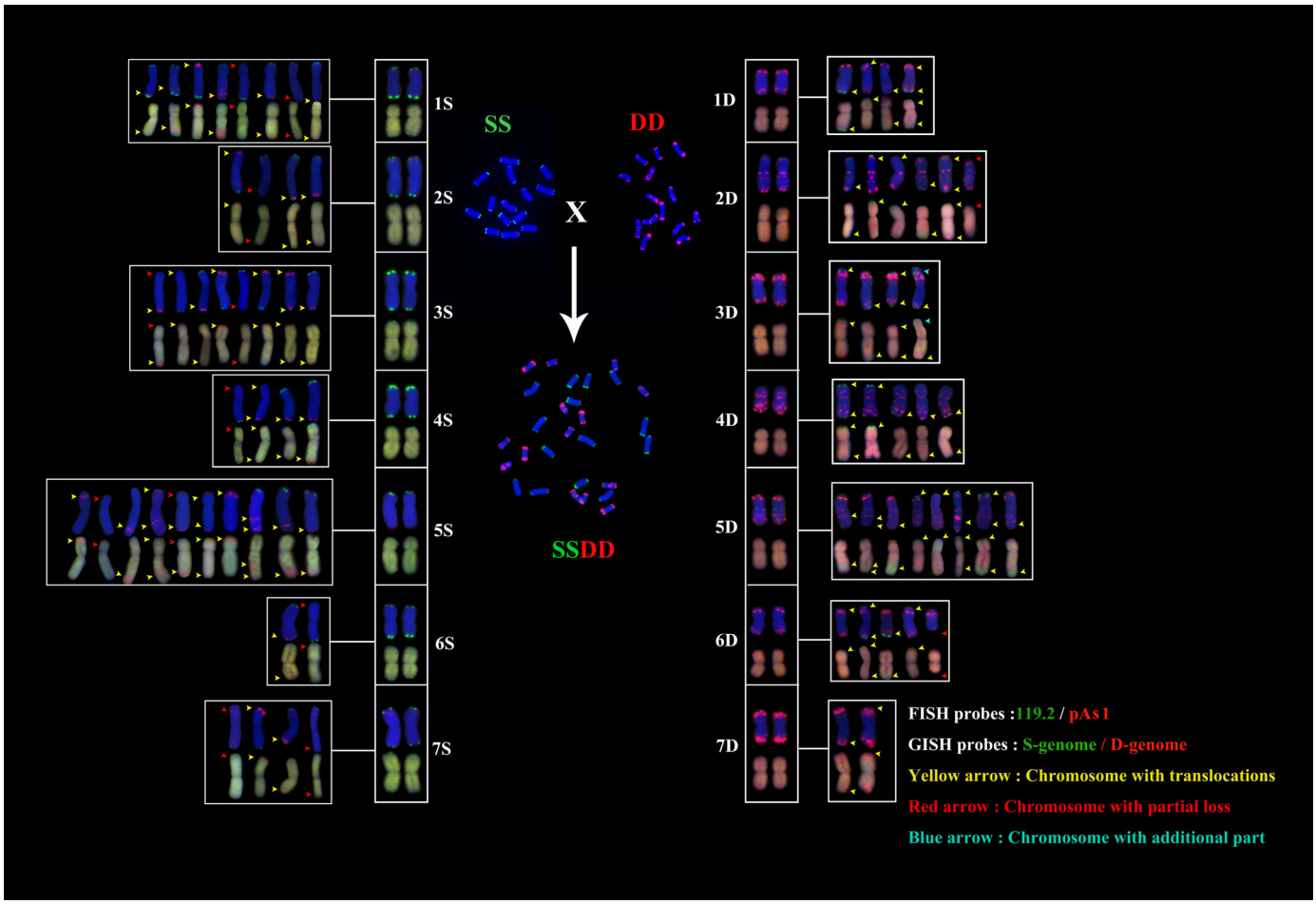

Fig. 3 Variable structural chromosome variations (SCVs) detected in population I (at S8) of the synthetic allotetraploid wheat (S^bS^bDD). The center images are standard fluorescence *in situ* hybridization (FISH) karyotypes of the diploid parents, *Aegilops bicornis* (S^bS^b) and *Aegilops tauschii* (DD), and an euploid individual of the synthetic allotetraploid (S^bS^bDD). Representative chromosomes of the S^b- and D-subgenomes with different SCVs detected by both FISH/genomic *in situ* hybridization (GISH) are shown. Yellow and red arrowheads denote translocations and chromosomes with large segmental loss, respectively. The pAs1 (red signals) and pSc119.2 (green signals) tandem DNA repeats were used as FISH probes. Genomic DNAs of *A. bicornis* (S^bS^b, green signals) and *A. tauschii* (DD, red signals) were used as GISH probes.

suggest functional compensation between the two kinds of chromosomal changes. To further investigate the relationship between NCVs and SCVs, and quantify differences of between-homoeolog compensation across the seven chromosome groups, we analyzed all plants that had a single monosomy/trisomy ('S^b chromosomes = 7 pairs + 1/D chromosomes = 7 pairs − 1' or 'S^b chromosomes = 7 pairs − 1/D chromosomes = 7 pairs + 1') or nullisomy/tetrasomy ('S^b chromosomes = 8 pairs/D chromosomes = 6 pairs' or 'S^b chromosomes = 6 pairs/D chromosomes = 8 pairs') numerical chromosomal constitutions (Fig. 5a), and tabulated the distribution of SCVs. We identified 243 individuals each containing a single monosomy/trisomy and 92 plants each containing a single nullisomy/tetrasomy constitution (Fig. 5b). First, for both monosomy/trisomy and nullisomy/tetrasomy, we found dramatic differences in the numbers of plants belonging to a specific homoeologous chromosome group (Fig. 5b). Specifically, for monosomy/trisomy, the largest number of plants ($n = 82$) showed group 5 homoeologous monosomy/trisomy ($5S^b/5D$), followed by homoeologous groups 2 ($n = 56$), 4 ($n = 39$), 3 ($n = 27$), 1 ($n = 26$), and 6 ($n = 10$) in a descending order, with group 7 homoeologous monosomy/trisomy category being represented by the smallest number of plants ($n = 3$; Fig. 5b). Broadly, the same tendency existed for nullisomy/tetrasomy, although the numbers of plants were smaller in each group, as expected (Fig. 5b). Second, for a given homoeologous chromosome pair, the S^b- and D-subgenome chromosomes were often asymmetric with respect to their likelihood to be in the monosomy/nullisomy vs trisomy/tetrasomy state (Fig. 5b). Specifically, for most of the homoeologous groups that had relatively large numbers of plants (i.e. homoeologous groups 5, 2, 3, and 1), the numbers of plants with S^b-subgenome chromosomes being in a trisomy/tetrasomy state was greater than those with D-subgenome chromosomes (Fig. 5b).

Another common feature in both the monosomy/trisomy and nullisomy/tetrasomy sets of plants was the common presence of SCVs on one or more of the chromosomes that were in the trisomy or tetrasomy state (Fig. 5a–d). Also, in the nullisomy/tetrasomy plants, the homoeologous compensating asymmetry

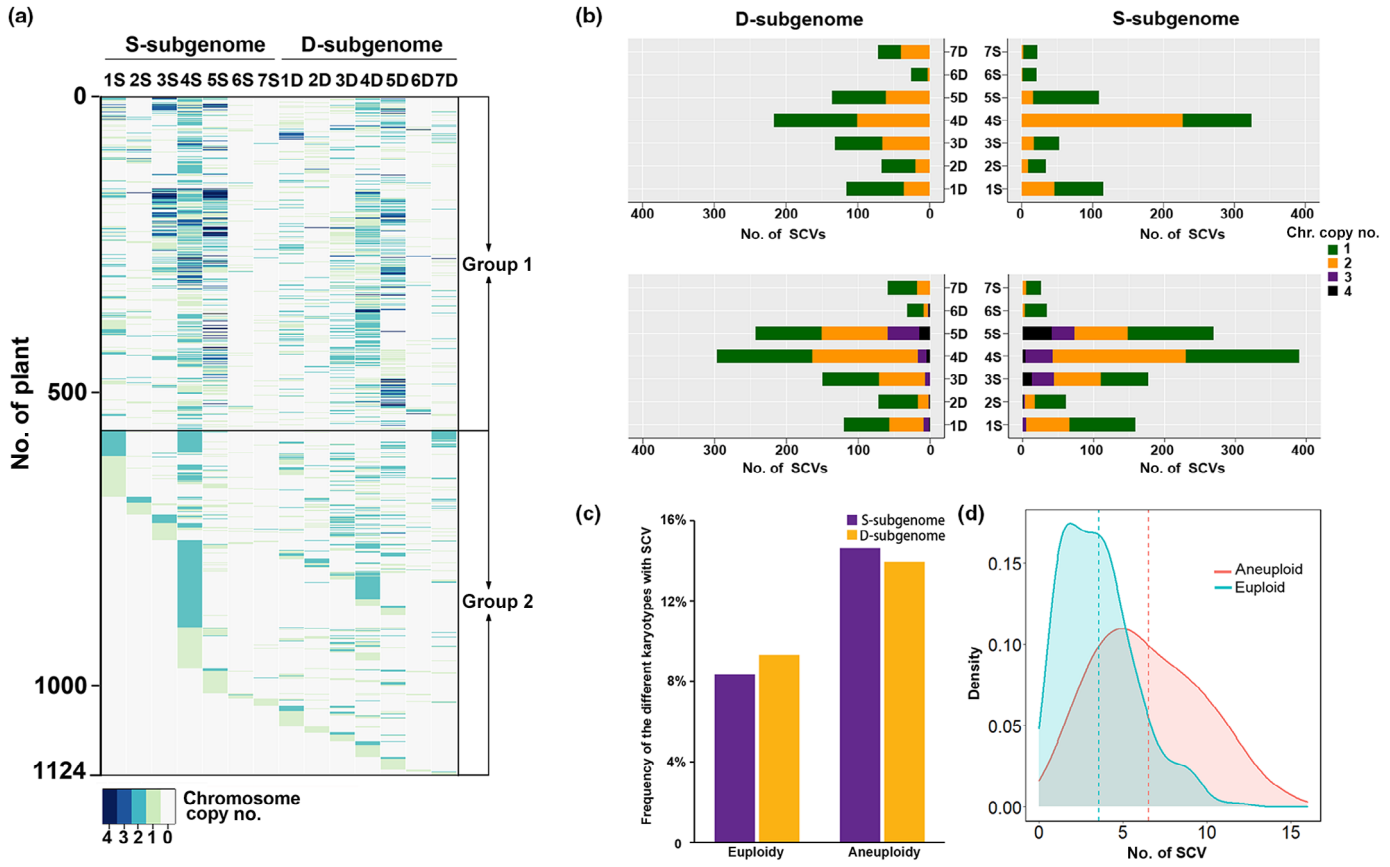

Fig. 4 Differences in frequencies of structural chromosome variations (SCVs) among chromosomes and between the two subgenomes in population I (at S8) of the synthetic allotetraploid wheat (S^bS^bDD). (a) Heatmap depicts SCVs among the 14 chromosomes of the S^b- and D-subgenomes of 1124 individuals that contained SCVs. Individuals showing SCVs are categorized into two groups: group I are euploid individuals with SCVs ($n = 587$) and group II are aneuploid individuals with SCVs ($n = 537$). Color key denotes chromosome copy numbers ranging from 0 to 4. (b) Bar graphs show relative proportions of SCVs between the S^b- and D-subgenome chromosomes of the groups I and II plants, respectively. The *x*-axis represents number of SCVs, and *y*-axis denotes the chromosomes. Color keys represent chromosome copy numbers ranging from 1 to 4. (c) Frequencies of SCVs in homoeologous chromosome groups 1–7 between the S^b- and D-subgenomes in the euploid and aneuploid plant groups, calculated by the formula 'no. of SCVs/total number of chromosomes/individuals'. (d) Density plot shows the distribution and mean of chromosomes with SCVs in euploid vs aneuploid plant groups. The *x*-axis represents the number of chromosomes with SCV in each of the individual plant, and the dashed lines in the middle were the mean of chromosomes with SCVs in the euploid and aneuploidy plant groups, respectively, which are significantly different (*t*-test: *P*-value = 6.026E-51).

appeared to be associated with the presence vs absence of SCVs, that is, for a given homoeologous chromosomal pair, the direction with a lower number (except for 0) of plants tended to have a higher percentage of plants with SCVs than the reciprocal direction with higher number of plants (Fig. 5b). In addition, in some of the $5S^b$/5D monosomy/ trisomy and nullisomy/tetrasomy plants two SCVs were detected on the same chromosome(s) in the same plant (Fig. 5a). Finally, more than one, and sometimes all, chromosomes in the trisomic or tetrasomic state harbored a SCV (Fig. 5c,d).

The foregoing observations collectively suggest a scenario whereby SCVs, by containing translocated segments from the otherwise missing chromosome(s), might contain subgenome-specific, essential genes that could not be efficiently compensated by the homoeologous chromosomes in the allotetraploid genetic background. Finally, with respect to fecundity (seed setting/individual), we found the compensation between group 5 homoeologous chromosomes was asymmetric, with trisomy 5D/monosomy $5S^b$ being significantly less fertile than that of trisomy $5S^b$/monosomy 5D (Fig. 5e). Fertilities of the remaining four homoeologous chromosome groups (1, 2, 4, and 6) did not significantly differ from each other. We also tested the extent of homoeologous compensation, that is, whether the compensated aneuploidies could reach the same fertility as euploids. We thus compared seed set of each of the trisomy/monosomy plant groups with the euploids. We found that seed set of three (i.e. trisomy 5D/monosomy $5S^b$, trisomy 2D/monosomy $2S^b$, and trisomy $2S^b$/monosomy 2D) of the eight plant groups was significantly lower than that in euploids, suggesting that homoeologous compensation was often insufficient to restore background fertility levels (Fig. 5e).

Meiotic irregularity and its correlation with chromosomal variation

We also constructed an independent population of synthetic allopolyploids (Fig. S2a) by selfing a S2 euploid plant sibling of the one giving rise to population I, described above, for 10 successive

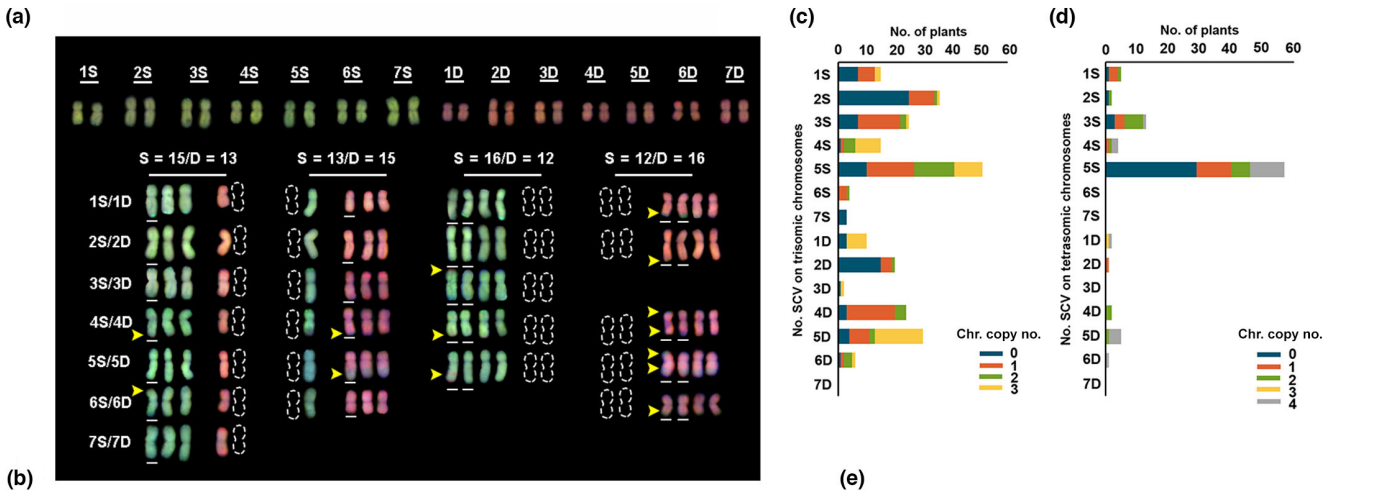

(b)

S = 3/D = 1	1S = 3/1D = 1	2S = 3/2D = 1	3S = 3/3D = 1	4S = 3/4D = 1	5S = 3/5D = 1	6S = 3/6D = 1	7S = 3/7D = 1
No. plant	16	36	25	15	51	4	3
No. and (%) plant with SCV	8 (50%)	11 (31%)	18 (75%)	14 (93%)	41 (80%)	4 (100%)	0 (0%)
D = 3/S = 1	1D = 3/1S = 1	2D = 3/2S = 1	3D = 3/3S = 1	4D = 3/4S = 1	5D = 3/5S = 1	6D = 3/6S = 1	7D = 3/7S = 1
No. plant	10	20	2	24	31	6	0
No. and (%) plant with SCV	8 (80%)	5 (25%)	1 (50%)	21 (88%)	27 (87%)	5 (83%)	0 (0%)
S = 4/D = 0	1S = 4/1D = 0	2S = 4/2D = 0	3S = 4/3D = 0	4S=4/4D = 0	5S = 4/5D = 0	6S = 4/6D = 0	7S = 4/7D = 0
No. plant	5	2	13	4	57	0	0
No. and (%) plant with SCV	4 (80%)	1 (50%)	10 (77%)	4 (100%)	28 (49%)	0 (0%)	0 (0%)
S = 0/D = 4	1D = 4/1S = 0	2D = 4/2S = 0	3D = 4/3S = 0	4D = 4/4S = 0	5D = 4/5S = 0	6D = 4/6S = 0	7D = 4/7S = 0
No. plant	2	1	0	2	5	1	0
No. and (%) plant with SCV	2 (100%)	1 (100%)	0 (0%)	2 (100%)	5 (100%)	1 (100%)	0 (0%)

(e)

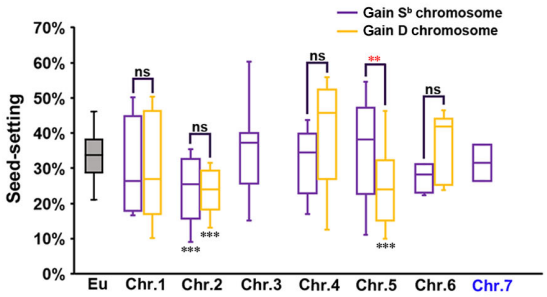

Fig. 5 Types and structural chromosome variation (SCV) frequencies of homoeologous chromosome pairs in compensated aneuploidy in population I (at S8) of the synthetic allotetraploid wheat (S^bS^bDD). (a) Trisomy/monosomy ($S^b = 15/D = 13$, $S^b = 13/D = 15$) and tetrasomy/nullisomy ($S^b = 16/D = 12$, $S^b = 12/D = 16$) of the seven sets of homoeologous chromosomes. The white horizontal line indicates the gain of chromosome and the dash-lined frames refer to loss of chromosomes. The yellow arrowheads denote location of SCVs. (b) The number of individuals with only one pair of homoeologous chromosomes as trisomy/monosomy or tetrasomy/nullisomy, and the number and proportion of SCVs contained by these plants. (c, d) The number of plants containing SCVs in each of the seven sets of homoeologous chromosomes in the trisomy/monosomy state (c) or the tetrasomy/nullisomy state (d). Color keys denote the number of plants with altered chromosome number (showing NCV) containing different numbers of SCVs in the variable chromosome, which varied from 0 to 4. (e) Homoeologous asymmetry in relation to seed setting/individual in each of the seven sets of homoeologous chromosomes in plants with trisomy/monosomy for a single homoeologous chromosome pair. The *x*-axis denotes the seven sets of homoeologous chromosomes; the gray box refers to euploidy. Chromosome 3 refers to precocious death (before maturity) of plants with a $3S^b$-monosomy/3D-trisomy karyotype. Chromosome 7 (in blue) refers to plant with a $7S^b$-monosomy/7D-trisomy karyotype was not identified in the analyzed plants. The bounds of the box are the first and third quartiles (Q1 and Q3). Whiskers represent data range, bounded to 1.5 × (Q3 − Q1). Statistical results above the bars refer to pairwise comparison in fertility between the reciprocal monosomy/trisomy plants, while those below the bars refer to comparisons the euploidy. Wilcoxon test: **, $P < 0.01$; ***, $P < 0.001$; ns, not significant.

generations and karyotyped a subset of progenies at each generation, whereby only euploid plants were selected to produce the next generation. This population thus represented a 'multigenerational euploidy-selecting pedigree' (population II; Fig. S2a). As expected, we found that the proportions of plants with NCVs and SCVs at each generation of this population were lower (Figs S2b–e, S4; Methods S1; Notes S1) than those of the population I that was propagated by selfing without karyotype selection at any intervening generation (Fig. 1). Specifically, we karyotyped a total of 487 individuals from population II (Fig. S2) and analyzed both NCVs and SCVs (Fig. S4; Methods S1; Notes S1). The general patterns of both NCVs and SCVs in population II were similar to those of population I. However, some discrepancies in NCVs were also evident. For example, the relative frequencies of NCVs of group 2 chromosomes were among the highest in population II (Fig. S4b), but which were among the average in population I (Fig. 2b). Nevertheless, the discrepancies could be readily accounted for by differences in their propagation between the two populations rather than entailing potential amplifying effects of certain outlier karyotypic variants in population I.

Given that no somatic mosaicism in NCV/SCV was found in the root-tip cells of any of the 1322 karyotyped plants (Fig. 1) nor of the euploidy-selected plants (Fig. S2), we infer that the chromosomal variations trace to meiotic irregularity rather than impaired mitosis. Because the rates of NCVs and SCVs were broadly constant across the different generations of euploid plants in this pedigree (Fig. S2a), this suggests that the extent of meiotic irregularity was largely constant among the euploid individuals from different generations.

Based on the above results, we randomly selected 10 euploid individuals from the S4 and S6 selfed generations (five individuals from each generation) of this pedigree (Fig. S2a), for meiotic analysis of pollen mother cells (PMCs) by combined GISH and FISH. We found that, indeed, the chromosome behavior at meiotic metaphase I (MI) among the PMCs of the 10 individuals was highly similar. On average, PMCs of each plant produced 12.7–13.1 homologous (homo)-bivalents, of which *c.* 80% were ring-shaped, while *c.* 20% were rod-shaped; the other 2–4 chromosomes showed irregular configurations, including quadrivalents, trivalents, heteromorphic (hetero-) bivalents, or univalents (Fig. 6a–e; Table S2). We found dramatic differences among the seven homoeologous chromosome groups in meiotic irregularities. Specifically, group 2 showed the highest proportions of all four types of irregular chromosomal configurations (quadrivalent, trivalent, hetero-bivalent, and univalent; Binomial test, all *P*-values < 0.001) while groups 6 and 7 showed the lowest (Binomial test, all *P*-values < 0.001), with the other groups being in-between (Fig. 6f; Table S2). We noted that homoeologous chromosomes within a given group (or pair) also varied in their propensities to form univalents (Fig. 6e; Table S2), which was probably due to their differences in forming trivalents, that is, in situations when a univalent and a trivalent of the same homoeologous chromosome group formed in a given MI but the two members varied with respect to being as univalent or trivalent.

We further tested contributions of the different types of irregular meiotic configurations (together or in separation) to the formation of organismal NCVs and SCVs, respectively, for plants in this population II (Fig. S2). For NCVs, we first tested correlation between the overall irregular meiotic configurations with NCVs, and found that the two variables showed a significant positive correlation (Pearson correlation coefficient $r = 0.94$, *P*-value = 0.0015; Fig. 7a). We then tested each type of the irregular meiotic configurations with NCVs and found that three of the four configuration types (quadrivalent, trivalent, and hetero-bivalent) were significantly positively correlated with NCVs ($r = 0.81$, 0.94, and 0.99, respectively; all *P*-values < 0.05; Fig. 7b–d), while univalent showed no correlation ($r = 0.40$, *P*-value = 0.38; Fig. 7e). Unexpectedly, we found no significant correlation between the irregular meiotic configurations and SCVs when all chromosomes were tabulated together; this was true either when all three types of configurations were considered together or separately for each of the three types (i.e. quadrivalent, trivalent, and hetero-bivalent; univalent was not relevant for assaying SCVs; Fig. S5). We noted, however, that group 2 chromosomes showed the highest frequencies of all three types of nonhomologous configurations (Fig. 6f). We thus suspected that group 2 chromosomes might be an outlier, which might have confounded an otherwise existing correlation. We calculated Cook's distance for each of the seven chromosome groups and found that group 2 was the only one with Cook's distance > 1 (Table S3), indicating it was indeed an outlier. As expected, when group 2 was excluded, the correlations between irregular meiotic configurations and organismal SCVs were significant both when all three types of configurations were tabulated together ($r = 0.93$, *P*-value = 0.0072) or each type in separation ($r = 0.84$, 0.75 and 0.92 for quadrivalent, trivalent, and heteromorphic bivalent, respectively; all *P*-values < 0.05; Fig. S5). Together, these results indicate that meiotic chromosomal irregularity was highly correlated with NCVs, and except for group 2 chromosomes, also with SCVs.

Homoeologous chromosome pairing is positively correlated with sequence synteny at the subtelomeric regions of both chromosome arms

In principle, the dramatic difference among homoeologous chromosome groups in their frequencies of forming multivalents and hetero-bivalents could be due to differential genetic divergence in sequence or in structure. We thus attempted to deconvolute the nature of the genetic affinity between homoeologous chromosomes that might have underpinned their meiotic pairing frequencies. We conducted comparative analyses between the S^b and D genomes of the parental species, *A. bicornis*, and *A. tauschii*, at multiple levels and calculated their correlations with homoeologous meiotic pairing irregularities. It is known that although the S^b and D genomes have markedly different genome sizes (5.64 and 3.95 Gb, respectively), they still maintain overall synteny and share high levels of nucleotide identity in genic regions (Li *et al.*, 2022). Our comparative analyses confirmed the genome size differences, with each of the seven *A. bicornis* chromosomes being substantially longer than their *A. tauschii* homoeologous counterparts (Fig. S6). We compared differences among the seven homoeologous chromosome groups with respect to overall synteny, genic synteny, genic similarity (percent nucleotide identity), structural variants, and content of transposable elements (TEs), and found substantial differences but similarly high levels of genic sequence identity among the homoeologous chromosome groups in these variables (Table S4). We also found large numbers of structural variants (SVs), including inversions and large segmental deletions/insertions causing presence/absence variations (PAVs) between each homoeologous chromosome pair, and which varied markedly among the seven homoeologous chromosome groups (Fig. S6). We next calculated the Pearson correlation coefficients between each of these variables and the overall homoeologous chromosome pairing irregularity, but found no significant correlation (Fig. S7). This suggests that, when entire chromosomes were considered, inter-homoeologous genetic differentiation in any of these features did not constitute a determinant or a major contributing factor to homoeologous chromosome pairing differences during meiosis.

We then tested the possibility that only specific chromosomal region(s) might contribute to homoeologous pairing, which might have been obscured in the full-chromosome comparisons. First, based on the distribution and density of genes and TEs, we delineated the proximal position of centromeres for each of the 14 pairs of homoeologous chromosomes (Figs 8a, S8). Then, starting from the boundaries of each of the defined centromeric regions, we partitioned each chromosome arm into 10, 15, and 20 equal-length (in nt) segments, and calculated the Pearson correlation coefficients between synteny of each segment (the centromeric region as a separate segment) with the overall homoeologous pairing irregularity. We found that only synteny levels of the most terminal segments (i.e. the subtelomeric

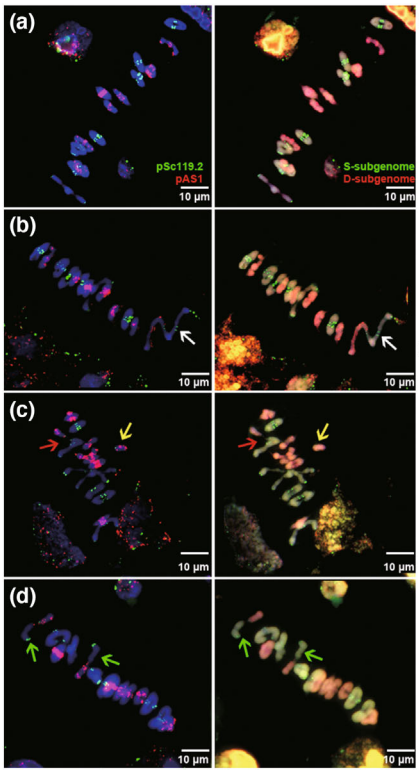

(e)

Plant	No. of PMCs at metaphase I	No. and (%) PMCs showing regular pairing	No. and (%) PMCs showing irregular pairing	Bivalent		No. of abnormal pairing events			
				Rod/PMC	Ring/PMC	Quadrivalent	Trivalent	Hetero-bivalent	Univalent
SSDD-1	45	26 (57.8)	19 (42.2)	2.42	10.69	7	2	4	16
SSDD-2	30	13 (43.3)	17 (56.7)	2.53	10.53	4	1	11	11
SSDD-3	42	21 (50.0)	21 (50.0)	2.17	10.62	12	1	15	14
SSDD-4	48	23 (47.9)	25 (52.1)	2.71	10.31	9	4	11	17
SSDD-5	20	11 (55.0)	9 (45.0)	2.2	10.5	4	3	8	9
SSDD-6	35	19 (54.3)	16 (45.7)	2.37	10.77	8	3	4	10
SSDD-7	42	24(57.1)	18(42.9)	2.60	10.26	15	0	11	10
SSDD-8	39	20 (51.3)	19 (48.7)	2.44	10.44	9	3	12	11
SSDD-9	34	15 (44.1)	19 (55.9)	2.71	10.09	8	2	11	16
SSDD-10	25	15 (60.0)	10(40.0)	2.12	10.96	7	3	0	6
Total	360	187 (51.9)	173 (48.1)	2.43	10.52	83 (26.4%)	22 (7.0%)	87 (27.7%)	122 (38.9%)

(f)

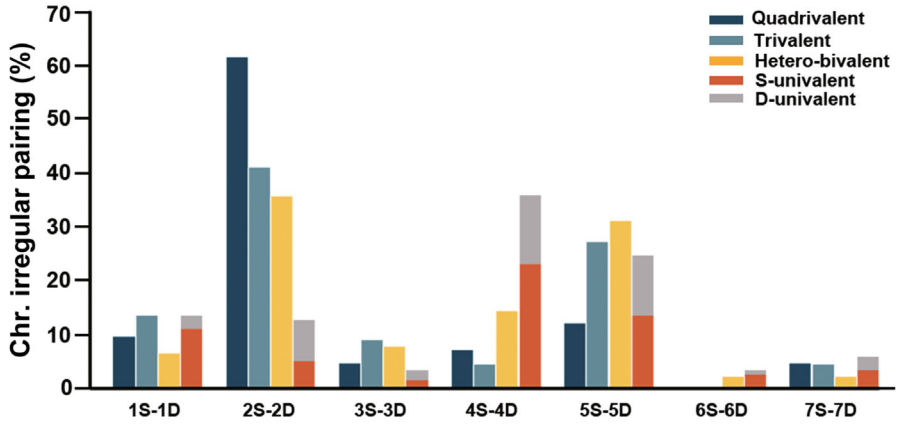

Fig. 6 Meiotic chromosome paring behavior at metaphase of meiosis I (MI) of pollen mother cells (PMCs) in euploid individuals of population II of the synthetic allotetraploid wheat (S^bS^bDD). (a–d) are representative fluorescence *in situ* hybridization (FISH)/genomic *in situ* hybridization (GISH) images of chromosome pairing behavior at MI of PMCs. (a) A plant with exclusive bivalent pairing by all 14 homologous chromosome pairs; (b) a plant with 12 bivalents and a quadrivalent (white arrow); (c) a plant with 12 bivalents plus a trivalent (red arrow) and a univalent (yellow arrow); (d) a plant with 12 bivalents and two hetero-bivalents (green arrows). The pAs1 (red signals) and pSc119.2 (green signals) tandem DNA repeats were used as FISH probes. Genomic DNAs of *Aegilops bicornis* (S^bS^b, green signals) and *Aegilops tauschii* (DD, red signals) were used as GISH probes. (e) Tabulated number and percent of chromosome pairing behavior at MI of PMCs of all 10 euploid plants. The 10 euploid individuals used for meiotic analysis were from S4 and S6 (five from each generation). (f) Percentages of the variable meiotic pairing irregularities (quadrivalents, trivalents, hetero-bivalents, and univalents) shown by each of the seven sets of homoeologous chromosomes.

regions) showed consistent correlations with homoeologous pairing irregularity in all three-length dissection categories while structural variation and genic sequence similarity did not, that is, which might show correlations in one or two window size(s) but never in all three (Figs S9–S12; Table S5). For example, in the 20 segments/arm analysis, the Pearson correlation coefficients between the two variables (synteny and homoeologous paring irregularity) were 0.8 (P-value = 0.032) for the short-arm and 0.75 (P-value = 0.053) for the long-arm, respectively (Fig. 8b,c). We further separately calculated the Pearson correlation coefficients of subtelomeric region synteny of both arms with each specific type of homoeologous pairing irregularity, that is, quadrivalents, trivalents, and hetero-bivalents. We found that subtelomeric region synteny in both arms showed clear signs of positive correlation with all three types of homoeologous pairing irregularity, but the correlations with quadrivalents were most significant, which were 0.88 (P-value = 0.008) and 0.81 (P-value = 0.026) for the short- and long-arm subtelomeric regions, respectively (Fig. S13).

The foregoing results suggest that degree of synteny in the subtelomeric regions is likely a major determinant of homoeologous chromosome pairing. We therefore analyzed whether differences in the degrees of between-homoeologous synteny would mirror the difference among the homoeologous chromosome pairs in their meiotic irregularity phenotypes. Indeed, we found that homoeologous chromosome pairs $2S^b$/2D and $5S^b$/5D, which manifested the highest percent of meiotic irregularity of all three types (quadrivalents, trivalents, and hetero-bivalents; Fig. 6), also had the highest levels of synteny at subtelomeric regions of both arms (Table S5). In parallel, homoeologous chromosome pairs $3S^b$/3D, $6S^b$/6D, and $7S^b$/7D, which manifested the lowest percent of meiotic irregularity of all three types (quadrivalents, trivalents, and hetero-bivalents; Fig. 6), had the lowest levels of synteny at the subtelomeric regions (Table S5). We need to point out, however, that the well-known telomere-bouquet structure during the commencement of meiotic pairing in grasses (Corredor *et al.*, 2007) may also be a contributing factor to the stronger correlation of distal regions with homoeologous meiotic pairing than other regions.

Impacts of numerical and structural chromosomal variation on phenotypes

Both numerical and structural chromosomal variation may cause profound changes in gene expression via *cis*- and *trans*-regulation,

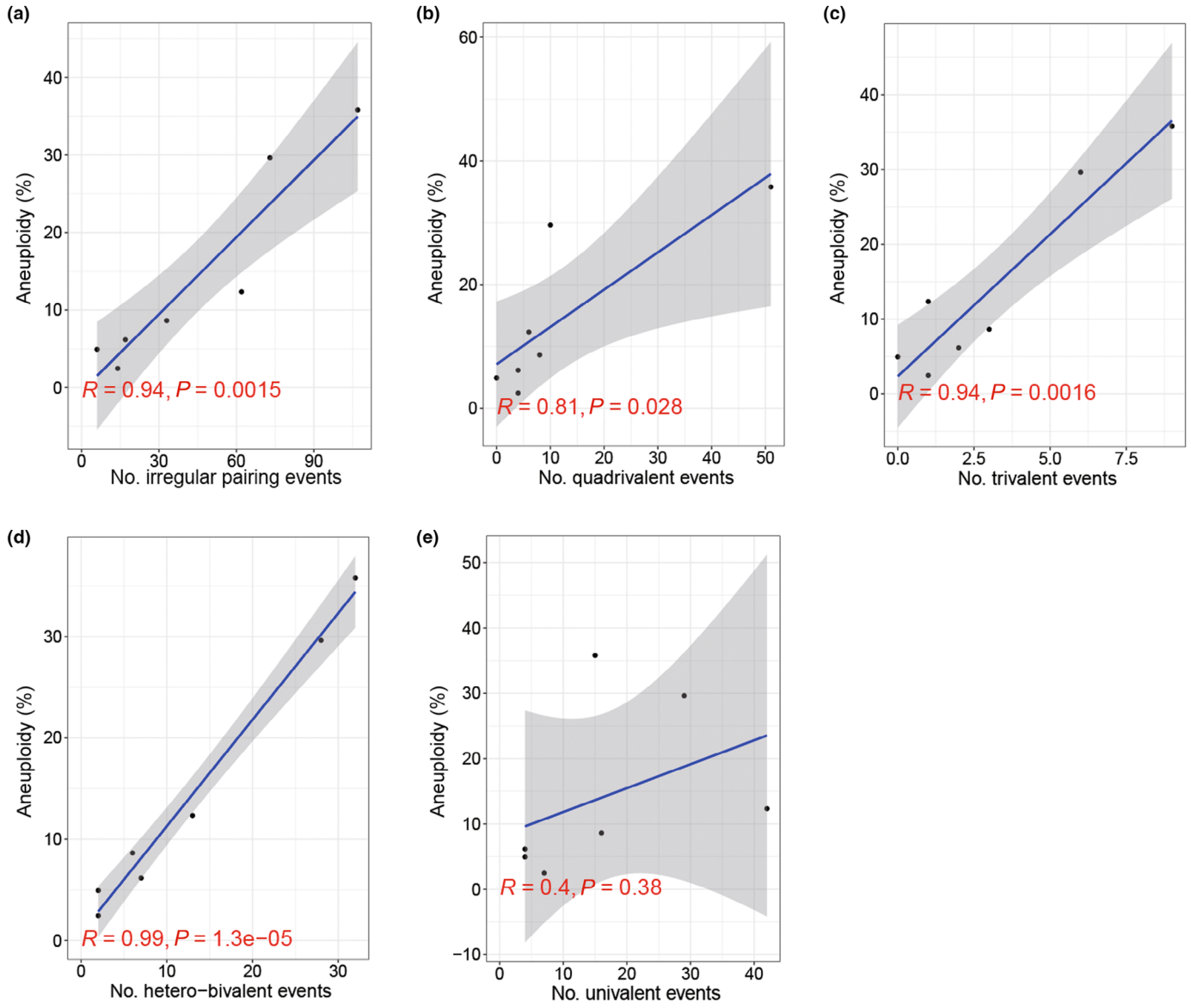

Fig. 7 Correlations between homoeologous chromosome pairing irregularities at meiosis I (MI) of pollen mother cells (PMCs) and numerical chromosome variants (NCVs) in population II of the synthetic allotetraploid wheat (S^bS^bDD). (a) Correlations between the overall amount of homoeologous chromosome pairing irregularity at MI and the frequencies of NCVs. (b–e) Correlations between the numbers of each type of homoeologous chromosome pairing irregularity, that is, quadrivalents, trivalents, hetero-bivalents, or univalents, and the frequencies of NCVs. Grey bands represent the 95% confidence interval bands. The data for homoeologous chromosome pairing irregularities and NCVs are all from the 'euploidy-selecting population'. Pearson correlation coefficients are shown.

due to gene dosage and other effects (Birchler & Veitia, 2012; Bottani *et al.*, 2018; Bao *et al.*, 2019; Hu & Wendel, 2019; Veitia & Birchler, 2022), thereby affecting phenotypes. To investigate the impact of NCVs and SCVs on phenotypes, we measured eight morphological traits related to growth, development, and reproductive fitness, that is, plant height, tiller number, spike length, spikelet number per spike, seed set, seed length, seed width, and one hundred-seed-weight, of the six plant groups with either, or both, NCVs or SCVs (Fig. 1). Visual inspection indicated that variation in some, although probably not all, of these eight traits existed among the plant groups (e.g. Fig. 9a). We further performed statistical analysis of the variation in each of these traits among the plant groups. Due to insufficient numbers of the two plant groups, 'compensated aneuploidy without SCVs' and 'noncompensated aneuploidy without SCVs', they were not included in the statistical analysis. Results showed that (1) except for tiller number and grain width, both the mean and the magnitude of variation in the three plant groups, 'euploidy', 'compensated aneuploidy with SCVs', and 'noncompensated aneuploidy with SCVs' were greater than those of the euploidy group, consistent with the fact that each of these groups contained NCVs and/or SCVs concerning different chromosomes or chromosomal segments (Fig. 1); (2) plant height of 'euploidy with SCVs' was significantly higher than that of the other three populations (Wilcoxon test, *P*-value = 7.68E-05, *P*-value = 3.35E-04, *P*-value = 2.23E-05), while that of 'noncompensated aneuploidy with SCVs' group

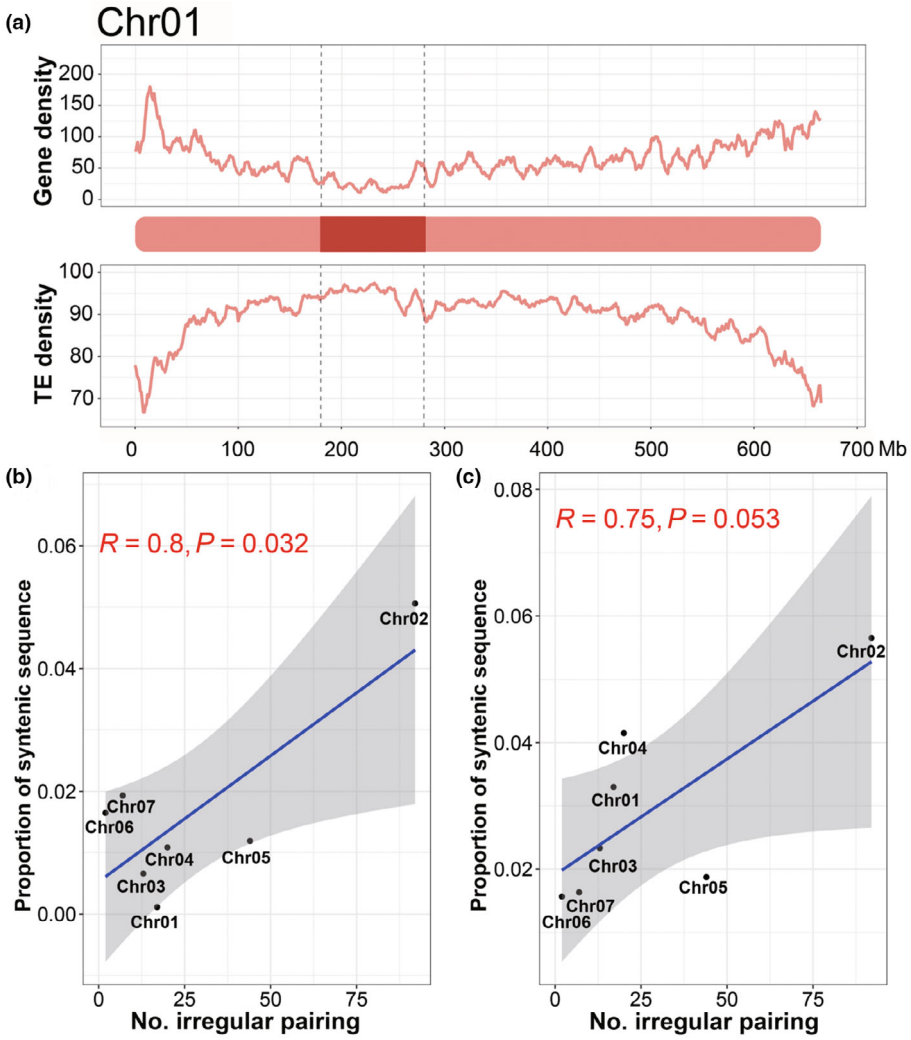

Fig. 8 Delineation of the centromere region of chromosome 1 based on the distribution densities of genes and transposable elements (TEs), and the correlations between subtelomeric sequence synteny and homoeologous chromosome pairing irregularity at meiosis I (MI) of pollen mother cells (PMCs). (a) Distribution of gene and TE densities along the entire length of chromosome 1, determined by methods as reported (Choulet *et al*., 2014). Data for all other chromosomes are presented in Supporting Information Fig. S8. A sliding window size of 10 Mb by step 1 Mb was used. The dashed lines represent the predicted start and end of the centromeric region. (b, c) Correlations between the degrees of subtelomeric sequence synteny of short- or long-arm with the numbers of homoeologous chromosome pairing irregularities at MI of PMCs. Grey bands represent the 95% confidence interval bands. The data for homoeologous chromosome pairing irregularities are from population II. Pearson correlation coefficients are shown.

was significantly lower than the other three groups (Wilcoxon test, *P*-value = 4.44E-02, *P*-value = 2.23E-05, *P*-value = 4.59E-03), but there was no difference between the '*bona fide* euploidy' and 'compensated aneuploidy with SCVs' groups (Wilcoxon test, *P*-value = 0.134); (3) no significant differences were detected in three traits (tiller number, one-hundred seed weight and grain width) between the euploidy and 'euploidy with SCVs' groups, but both groups showed significantly greater values than did the 'compensated aneuploidy with SCVs' and 'noncompensated aneuploidy with SCVs' groups; (4) there was no difference in seed set between the euploidy and 'compensated aneuploidy with SCVs' groups (Wilcoxon test, *P*-value = 0.343), but euploidy was significantly higher than the 'euploidy with SCVs' group (Wilcoxon test, *P*-value = 0.183E-02), while the 'noncompensated aneuploidy with SCVs' group was substantially less fertile (Wilcoxon test, *P*-value = 9.18E-04, *P*-value = 2.95E-02, *P*-value = 3.82E-02); and (5) difference existed in seed-width but not in seed-length among the plant groups, suggesting the former was causal to one-hundred seed weight difference, although variable degrees of grain-filling may also play a part (Fig. 9b). Together, these results indicate that both NCV and SCV had phenotypic consequences, and their co-occurrence further amplified phenotypic variation in the synthetic allotetraploid wheats, consistent with prior studies in other synthetic plant allopolyploids (e.g. Nicolas *et al*., 2012; Ferreira de Carvalho *et al*., 2021).

Discussion

Polyploidy is widely recognized as a pervasive force in biological evolution (Adams & Wendel, 2005; Comai, 2005; Chen, 2007; Otto, 2007; Soltis & Soltis, 2009; Wendel, 2015; Barker *et al*., 2016; Van de Peer *et al*., 2017), with allopolyploids, in particular, creating the opportunity for massive genomic and hence evolutionary novelty (Doyle *et al*., 2008). The mechanisms by which this new combinatorial complexity is generated become a matter of great interest, with considerable focus on genomic and genetic processes that might generate innovation (Adams & Wendel, 2005; Comai, 2005; Chen, 2007; Otto, 2007; Soltis *et al*., 2015; Wendel, 2015; Van de Peer *et al*., 2017; Bomblies, 2020). Here, we use an experimentally tractable system to study one aspect of this diversification, that is, rapid karyotypic

diversification in the immediate generations following allopolyploid formation in wheat. Numerous authors have pointed to 'genome shock' (McClintock, 1984; Dickinson *et al.*, 2003; Otto, 2007; Ha *et al.*, 2009; Buggs Richard *et al.*, 2011; Mandáková *et al.*, 2019) during the initial stages of allopolyploid formation as important in the generation of heritable variation that may fuel rapid evolutionary changes and facilitate establishment of nascent allopolyploid populations (Ramsey & Schemske, 2002; Soltis *et al.*, 2015; Van de Peer *et al.*, 2017; Wendel *et al.*, 2018).

Among the myriad genetic/epigenetic mechanisms comprising 'genome shock' in newly formed allopolyploids, those involving meiosis and chromosomal recombination are particularly relevant to the present study (Wendel, 2015; Lloyd & Bomblies, 2016; Bomblies, 2020; Addo Nyarko & Mason, 2022; Gonzalo, 2022). Nonhomologous chromosome pairing and recombination are known to stimulate genome restructuring and karyotypic diversification, in the process generating profound genetic and phenotypic consequences (Stebbins, 1951; Levin, 2002; Ramsey & Schemske, 2002; Bomblies, 2020). Homoeologous exchange (HE) resulting from homoeologous chromosome pairing and recombination (Gaeta & Chris Pires, 2010; Mason & Wendel, 2020) has been shown as an important mechanism generating genetic diversity in naturally formed neoallopolyploid species (Sybenga, 1996; Gaeta & Chris Pires, 2010; Chester *et al.*, 2012; Chalhoub *et al.*, 2014; Hollister, 2015; Mercier *et al.*, 2015; Bomblies *et al.*, 2016; Stein *et al.*, 2017; Hurgobin *et al.*, 2018; Lloyd *et al.*, 2018; Wang *et al.*, 2019). Nonetheless, allopolyploid species formed *in natura* are less than ideal for understanding the direct effects and consequences of karyotypic changes, because these are rarely 'caught in the act' and hence represent merely the survivors of past generative processes (Ramsey & Schemske, 2002). Moreover, natural allopolyploid species usually possess fully stabilized karyotypes, and hence, there is no real 'control' for comparison. By contrast, synthetic allopolyploids are model systems to assess the direct effects and immediate biological consequences of allopolyploidization-incurred genome shock (Ramsey & Schemske, 2002; Xiong *et al.*, 2011; Gaebelein *et al.*, 2019; Ferreira de Carvalho *et al.*, 2021; Shimizu, 2022; Zhang *et al.*, 2022). This is because evolution is yet to happen in synthetic allopolyploids, and the same population contains both karyotypically variable and invariable individuals for straightforward comparison.

We reported previously that synthetic allotetraploid wheats constructed by hybridizing diploid species of the *Aegilops–Triticum* complex showed high levels of meiotic perturbation and generated rampant karyotypic diversity (Gou *et al.*, 2018; Lv *et al.*, 2022). A notable observation from these prior studies is the substantial differences among the chromosomes in both types

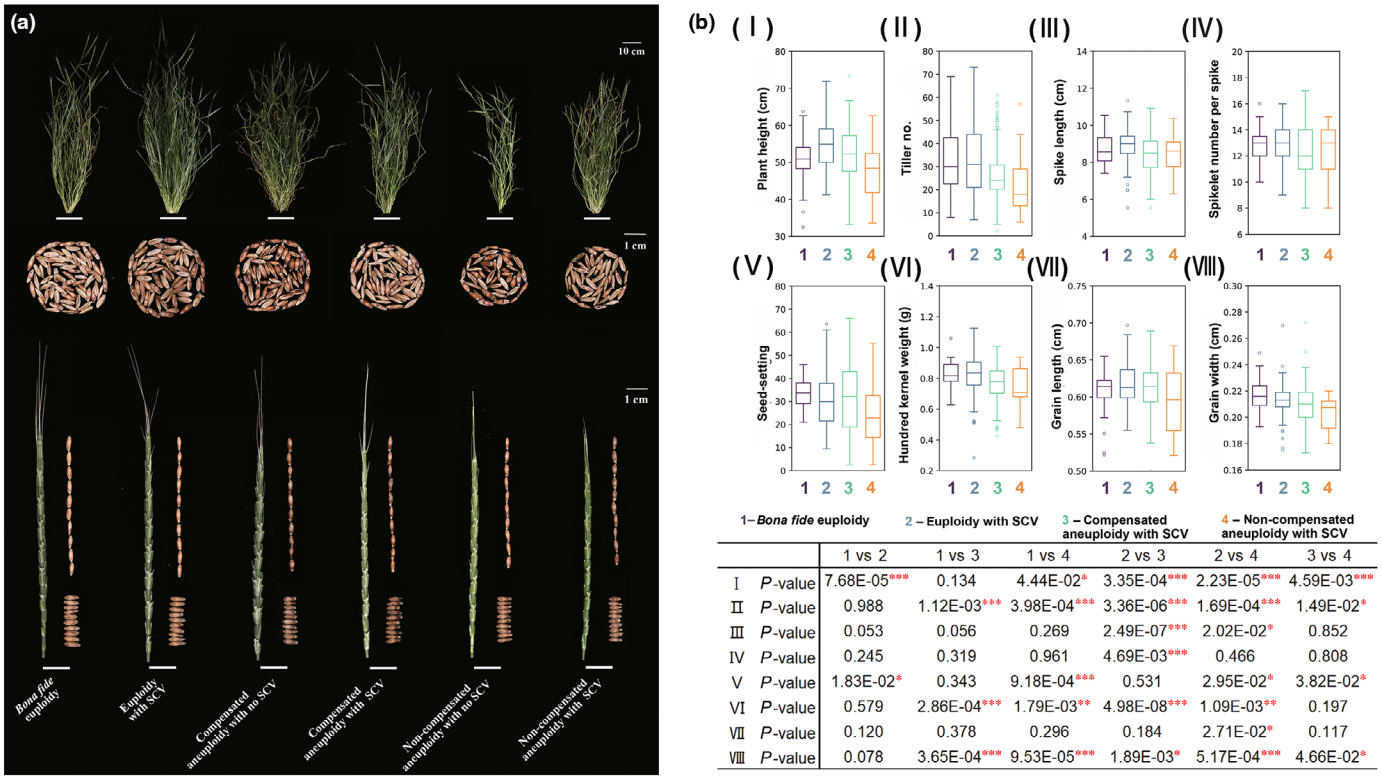

		1 vs 2	1 vs 3	1 vs 4	2 vs 3	2 vs 4	3 vs 4
Ⅰ	*P*-value	7.68E-05***	0.134	4.44E-02*	3.35E-04***	2.23E-05***	4.59E-03***
Ⅱ	*P*-value	0.988	1.12E-03***	3.98E-04***	3.36E-06***	1.69E-04***	1.49E-02*
Ⅲ	*P*-value	0.053	0.056	0.269	2.49E-07***	2.02E-02*	0.852
Ⅳ	*P*-value	0.245	0.319	0.961	4.69E-03***	0.466	0.808
Ⅴ	*P*-value	1.83E-02*	0.343	9.18E-04***	0.531	2.95E-02*	3.82E-02*
Ⅵ	*P*-value	0.579	2.86E-04***	1.79E-03**	4.98E-08***	1.09E-03**	0.197
Ⅶ	*P*-value	0.120	0.378	0.296	0.184	2.71E-02*	0.117
Ⅷ	*P*-value	0.078	3.65E-04***	9.53E-05***	1.89E-03*	5.17E-04***	4.66E-02*

Fig. 9 Effects of karyotype variation due to numerical chromosome variants (NCVs) and/or structural chromosome variations (SCVs) on phenotypes in the synthetic allotetraploid wheat (S^bS^bDD). (a) Examples of overall plant architecture, spike and seed morphology and seed setting of the six karyotype groups. (b) Quantification of eight morphological traits of four karyotypic groups. The eight traits are: plant height (I), tiller number (II), spike length (III), spikelet number per spike (IV), seed setting per plant (V), one hundred kernel weight (VI), grain length (VII), and grain width (VIII). The bounds of the box are the first and third quartiles (Q1 and Q3). Whiskers represent data range, bounded to 1.5 × (Q3 − Q1). Wilcoxon tests were used to test the statistical difference in each of the traits among the four karyotype groups; significant statistical differences are denoted as: *, $P < 0.05$; **, $P < 0.01$; ***, $P < 0.001$. All data are from population I.

and frequencies of NCVs and SCVs, consistent with studies in other neoallopolyploid plants (Nicolas *et al.*, 2009; Xiong *et al.*, 2011; Leal-Bertioli *et al.*, 2015; Chen *et al.*, 2018). However, none of these prior studies have addressed two critical questions: First, what are the determinant factors that underlie the dramatic differences among the chromosomes in their different propensities to undergo homoeologous pairing and recombination? Second, are there factors other than homoeologous pairing, such as differences in compensation between homoeologues, that also contribute to the variable frequencies of NCV and SCV manifested among the chromosomes? Focusing on these two questions constitutes the novel contribution of the current study.

Here, we constructed two populations of a synthetic allotetraploid wheat specifically suited to study this phenomenon. In population I, initiated from a single euploid individual that was propagated for eight successive generations without intervening selection, we assessed the amount, type, and spectrum of NCVs and SCVs that accumulate with each generation. In population II, using only euploid plants with selection for euploidy across the generations, we evaluated potential differences of euploid plants over time, investigated chromosome pairing behavior at meiosis. These two populations complement each other and allow the delineation of relationships between meiotic pairing irregularity and organismal karyotype variation, and also inform causations for meiotic pairing irregularity.

We show that all three types of meiotic chromosomal irregularity (quadrivalents, trivalents, and hetero-bivalents) were highly correlated with NCVs, and, except for group 2 homoeologous chromosomes, also with SCVs, confirming that all organismal karyotypic variants are derived from perturbed meiosis in synthetic allotetraploid wheat. We note, however, that the relationships between the two variables (meiotic irregularity and organismal NCVs/SCVs) are nonlinear, pointing to additional causative factors. We show that differential compensating capacities among the homoeologous chromosomes pairs is one such factor. This is evidenced by the strikingly different proportions of plants showing monosomy/trisomy and nullisomy/tetrasomy among the homoeologous chromosome groups and the asymmetry with respect to monosomy/nullisomy vs trisomy/tetrasomy between members of a given homoeologous chromosome pair. For homoeologous asymmetry, S^b-subgenome chromosomes were more often in a trisomy/tetrasomy state, suggesting they have a stronger compensating capacity for the loss of the corresponding D-subgenome homoeologous chromosomes than the reverse. We show that one constraint underlying homoeologous asymmetry is reproductive fitness, but it is conceivable that maintaining genome function may constitute another constraint, a possibility that needs further study. We need to point out that both the NCVs and SCVs we captured are likely only a portion of that generated due to possible constraints of gametic and/or saprophytic nonviability. Moreover, certain earlier karyotypic variants may have been disproportionately over-precipitated in later generations. Therefore, the karyotypic diversity we revealed more reflecting probabilistic than deterministic instant outcomes of allopolyploidization.

An important insight from the revolutionary progress made in genomic studies is the realization that all contemporary diploid species are rediploidized paleopolyploids (Li *et al.*, 2021). This suggests that the creative roles of WGD not only lie in gain of genetic material but also in selective loss (Albalat & Cañestro, 2016). Accumulated studies indicate that the rediploidization fractionation process often is asymmetric between subgenomes, with the dominant subgenome often less fractionated than the alternative, co-resident subgenome (Freeling *et al.*, 2015; Cheng *et al.*, 2018; Wendel *et al.*, 2018). Remarkably, subgenomic asymmetry can emerge and manifest immediately after allopolyploid formation (Edger *et al.*, 2017). Our results suggest that compensation asymmetry between homoeologous chromosome pairs with respect to their loss and gain in conferring reproductive fitness may predispose the genomic patterns and outcomes of diploidization in allopolyploids. This is consistent with observations in a synthetic *Brassica* allohexaploid (AABBCC), in which only a C-subgenome fragment replaces its counterpart of the A-subgenome, but not the reverse, affected fertility (Gaebelein *et al.*, 2019).

One of the most interesting findings, in our view is the demonstration that sequence synteny, rather than genic nucleotide similarly, in the subtelomeric regions was significantly correlated with meiotic chromosome pairing irregularity. This not only points to homoeologous chromosome pairing as the major mechanism of genome instability, but opens a window into exploring the responsible molecular genetic and chromatin level mechanisms (Morgan *et al.*, 2020). We should caution, however, that the correlations we detected are the aggregated results of all seven homoeologous chromosome pairs, as such, we cannot rule out the possibility that some pairs may not show such a correlation. Future studies by using a set of related synthetic allopolyploids would enable tabulating the correlations of each homoeologous chromosome pair in separation. Homoeologous chromosome pairing, a major type of allosyndetic pairing, is a double-edged sword: on one hand, it may generate homoeologous exchanges (HEs) that are 'useful' in a phenotypic sense and hence may become adaptive (Lloyd *et al.*, 2018; Mason & Wendel, 2020; Wu *et al.*, 2021; Wang *et al.*, 2022); on the other hand, the accumulation of HEs in a 'ratchet-like' fashion (Gaeta & Chris Pires, 2010) may further reduce inherent genetic differentiation between homoeologous chromosomes, and therefore obstruct the route to cytological diploidization. Conceivably, a novel genetic control mechanism, for example, the *Ph1* locus in polyploid wheat (Riley & Chapman, 1958; Sears, 1976; Griffiths *et al.*, 2006; Serra *et al.*, 2021) and the *PrBn* locus in *Brassica napus* (Jenczewski *et al.*, 2003; Nicolas *et al.*, 2009) via either *de novo* genetic mutation or introgression (Marburger *et al.*, 2019) is likely essential to enable meiotic stabilization of newly formed allopolyploid genomes (Bomblies *et al.*, 2016).

We show that phenotypic consequences of both NCVs and SCVs in the synthetic allotetraploid wheat were largely negative, that is, that they resulted in fitness reduction. This is as expected given that the assessment was performed in a permissive

laboratory environment without natural selection. It is conceivable that under adverse conditions, plants with specific NCVs and SCVs may show better performance, as documented by accumulating studies in both cellular and organismal contexts (Selmecki *et al.*, 2015; Zhu *et al.*, 2018; Wang *et al.*, 2022).

Acknowledgements

We are grateful to Prof. Moshe Feldman of the Weizmann Institute of Science, Israel, for providing the initial seeds used in this study, and to all three anonymous reviewers for their constructive comments. This work was supported by the National Natural Science Foundation of China (31991211) and an Israel Science Foundation (ISF)-China National Natural Science Foundation (NSFC) collaborative grant (32061143001).

Competing interests

None declared.

Author contributions

BL, CX and JFW designed the research. JZ constructed all the plant materials. JL, RL, BW and HX collected the plant materials and conducted phenotyping. JZ, TY and SL performed the cytogenetic analyses. JZ, JL, ZZ and CX completed comparative genomic analysis and correlation analyses. JZ, CX, JFW and BL wrote the manuscript with input from all authors. All authors read and approved the final manuscript. JZ and JL contributed equally to this work.

ORCID

Juzuo Li https://orcid.org/0000-0002-7771-3530
Bao Liu https://orcid.org/0000-0001-5481-1675
Ruili Lv https://orcid.org/0000-0002-9361-9413
Jonathan F. Wendel https://orcid.org/0000-0003-2258-5081
Chunming Xu https://orcid.org/0000-0002-0986-0993
Jing Zhao https://orcid.org/0000-0001-9716-8536

Data availability

Data are available in the article's Supporting Information.

References

Adams KL, Wendel JF. 2005. Polyploidy and genome evolution in plants. *Current Opinion in Plant Biology* **8**: 135–141.

Addo Nyarko C, Mason AS. 2022. Non-homologous chromosome pairing: sequence similarity or genetic control? *Trends in Genetics* **38**: 419–421.

Albalat R, Cañestro C. 2016. Evolution by gene loss. *Nature Reviews Genetics* **17**: 379–391.

Bao Y, Hu G, Grover CE, Conover J, Yuan D, Wendel JF. 2019. Unraveling *cis* and *trans* regulatory evolution during cotton domestication. *Nature Communications* **10**: 5399.

Barker MS, Husband BC, Pires JC. 2016. Spreading Winge and flying high: the evolutionary importance of polyploidy after a century of study. *American Journal of Botany* **103**: 1139–1145.

Birchler JA, Veitia RA. 2012. Gene balance hypothesis: connecting issues of dosage sensitivity across biological disciplines. *Proceedings of the National Academy of Sciences, USA* **109**: 14746–14753.

Bomblies K. 2020. When everything changes at once: finding a new normal after genome duplication. *Proceedings of the Royal Society B: Biological Sciences* **287**: 20202154.

Bomblies K, Jones G, Franklin C, Zickler D, Kleckner N. 2016. The challenge of evolving stable polyploidy: could an increase in "crossover interference distance" play a central role? *Chromosoma* **125**: 287–300.

Bottani S, Zabet NR, Wendel JF, Veitia RA. 2018. Gene expression dominance in allopolyploids: hypotheses and models. *Trends in Plant Science* **23**: 393–402.

Buggs Richard JA, Zhang L, Miles N, Tate Jennifer A, Gao L, Wei W, Schnable Patrick S, Barbazuk WB, Soltis Pamela S, Soltis Douglas E. 2011. Transcriptomic shock generates evolutionary novelty in a newly formed, natural allopolyploid plant. *Current Biology* **21**: 551–556.

Chalhoub B, Denoeud F, Liu S, Parkin IAP, Tang H, Wang X, Chiquet J, Belcram H, Tong C, Samans B *et al.* 2014. Early allopolyploid evolution in the post-Neolithic *Brassica napus* oilseed genome. *Science* **345**: 950–953.

Chen S, Ren F, Zhang L, Liu Y, Chen X, Li Y, Zhang L, Zhu B, Zeng P, Li Z *et al.* 2018. Unstable allotetraploid tobacco genome due to frequent homeologous recombination, segmental deletion, and chromosome loss. *Molecular Plant* **11**: 914–927.

Chen ZJ. 2007. Genetic and epigenetic mechanisms for gene expression and phenotypic variation in plant polyploids. *Annual Review of Plant Biology* **58**: 377–406.

Cheng F, Wu J, Cai X, Liang J, Freeling M, Wang X. 2018. Gene retention, fractionation and subgenome differences in polyploid plants. *Nature Plants* **4**: 258–268.

Chester M, Gallagher J, Symonds V, Silva AV, Mavrodiev E, Leitch A, Soltis P, Soltis D. 2012. Extensive chromosomal variation in a recently formed natural allopolyploid species, *Tragopogon miscellus* (Asteraceae). *Proceedings of the National Academy of Sciences, USA* **109**: 1176–1181.

Choulet F, Alberti A, Theil S, Glover N, Barbe V, Daron J, Pingault L, Sourdille P, Couloux A, Paux E *et al.* 2014. Structural and functional partitioning of bread wheat chromosome 3B. *Science* **345**: 1249721.

Comai L. 2005. The advantages and disadvantages of being polyploid. *Nature Reviews Genetics* **6**: 836–846.

Corredor E, Lukaszewski AJ, Pachón P, Allen DC, Naranjo TS. 2007. Terminal regions of wheat chromosomes select their pairing partners in meiosis. *Genetics* **177**: 699–706.

Dickinson HG, Hiscock SJ, Crane PR, Comai L, Madlung A, Josefsson C, Tyagi A. 2003. Do the different parental 'heteromes' cause genomic shock in newly formed allopolyploids? *Philosophical Transactions of the Royal Society of London. Series B: Biological Sciences* **358**: 1149–1155.

Doyle JJ, Flagel LE, Paterson AH, Rapp RA, Soltis DE, Soltis PS, Wendel JF. 2008. Evolutionary genetics of genome merger and doubling in plants. *Annual Review of Genetics* **42**: 443–461.

Edger PP, Smith R, McKain MR, Cooley AM, Vallejo-Marin M, Yuan Y, Bewick AJ, Ji L, Platts AE, Bowman MJ *et al.* 2017. Subgenome dominance in an interspecific hybrid, synthetic allopolyploid, and a 140-year-old naturally established neo-allopolyploid monkeyflower. *Plant Cell* **29**: 2150–2167.

Feldman M, Levy AA. 2012. Genome evolution due to allopolyploidization in wheat. *Genetics* **192**: 763–774.

Feldman M, Levy AA, Fahima T, Korol A. 2012. Genomic asymmetry in allopolyploid plants: wheat as a model. *Journal of Experimental Botany* **63**: 5045–5059.

Ferreira de Carvalho J, Stoeckel S, Eber F, Lodé-Taburel M, Gilet M-M, Trotoux G, Morice J, Falentin C, Chèvre A-M, Rousseau-Gueutin M. 2021. Untangling structural factors driving genome stabilization in nascent *Brassica napus* allopolyploids. *New Phytologist* **230**: 2072–2084.

Freeling M, Scanlon MJ, Fowler JE. 2015. Fractionation and subfunctionalization following genome duplications: mechanisms that drive gene content and their consequences. *Current Opinion in Genetics & Development* **35**: 110–118.

Gaebelein R, Schiessl SV, Samans B, Batley J, Mason AS. 2019. Inherited allelic variants and novel karyotype changes influence fertility and genome stability in *Brassica* allohexaploids. *New Phytologist* **223**: 965–978.

Gaeta RT, Chris Pires J. 2010. Homoeologous recombination in allopolyploids: the polyploid ratchet. *New Phytologist* **186**: 18–28.

Glémin S, Scornavacca C, Dainat J, Burgarella C, Viader V, Ardisson M, Sarah G, Santoni S, David J, Ranwez V. 2019. Pervasive hybridizations in the history of wheat relatives. *Science Advances* **5**: eaav9188.

Goel M, Sun H, Jiao W-B, Schneeberger K. 2019. SyRI: finding genomic rearrangements and local sequence differences from whole-genome assemblies. *Genome Biology* **20**: 277.

Gonzalo A. 2022. All ways lead to Rome-meiotic stabilization can take many routes in nascent polyploid plants. *Genes* **13**: 147.

Gou X, Bian Y, Zhang A, Zhang H, Wang B, Lv R, Li J, Zhu B, Gong L, Liu B. 2018. Transgenerationally precipitated meiotic chromosome instability fuels rapid karyotypic evolution and phenotypic diversity in an artificially constructed allotetraploid wheat (AADD). *Molecular Biology and Evolution* **35**: 1078–1091.

Griffiths S, Sharp R, Foote TN, Bertin I, Wanous M, Reader S, Colas I, Moore G. 2006. Molecular characterization of *Ph1* as a major chromosome pairing locus in polyploid wheat. *Nature* **439**: 749–752.

Ha M, Lu J, Tian L, Ramachandran V, Kasschau KD, Chapman EJ, Carrington JC, Chen X, Wang X-J, Chen ZJ. 2009. Small RNAs serve as a genetic buffer against genomic shock in *Arabidopsis* interspecific hybrids and allopolyploids. *Proceedings of the National Academy of Sciences, USA* **106**: 17835–17840.

Han F, Liu B, Fedak G, Liu Z. 2004. Genomic constitution and variation in five partial amphiploids of wheat–*Thinopyrum* intermedium as revealed by GISH, multicolor GISH and seed storage protein analysis. *Theoretical and Applied Genetics* **109**: 1070–1076.

Hollister JD. 2015. Polyploidy: adaptation to the genomic environment. *New Phytologist* **205**: 1034–1039.

Hu G, Wendel JF. 2019. *Cis–trans* controls and regulatory novelty accompanying allopolyploidization. *New Phytologist* **221**: 1691–1700.

Hurgobin B, Golicz AA, Bayer PE, Chan C-KK, Tirnaz S, Dolatabadian A, Schiessl SV, Samans B, Montenegro JD, Parkin IAP *et al.* 2018. Homoeologous exchange is a major cause of gene presence/absence variation in the amphidiploid *Brassica napus*. *Plant Biotechnology Journal* **16**: 1265–1274.

Jenczewski E, Eber F, Grimaud A, Huet S, Lucas MO, Monod H, Chèvre AM. 2003. *PrBn*, a major gene controlling homeologous pairing in oilseed rape (*Brassica napus*) haploids. *Genetics* **164**: 645–653.

Jiao Y, Wickett NJ, Ayyampalayam S, Chanderbali AS, Landherr L, Ralph PE, Tomsho LP, Hu Y, Liang H, Soltis PS *et al.* 2011. Ancestral polyploidy in seed plants and angiosperms. *Nature* **473**: 97–100.

Jighly A, Joukhadar R, Sehgal D, Singh S, Ogbonnaya FC, Daetwyler HD. 2019. Population-dependent reproducible deviation from natural bread wheat genome in synthetic hexaploid wheat. *The Plant Journal* **100**: 801–812.

Kashkush K, Feldman M, Levy A. 2002. Gene loss, silencing and activation in a newly synthesized wheat allotetraploid. *Genetics* **160**: 1651–1659.

Kato A, Lamb JC, Birchler JA. 2004. Chromosome painting using repetitive DNA sequences as probes for somatic chromosome identification in maize. *Proceedings of the National Academy of Sciences, USA* **101**: 13554–13559.

Kenan-Eichler M, Leshkowitz D, Tal L, Noor E, Melamed-Bessudo C, Feldman M, Levy AA. 2011. Wheat hybridization and polyploidization results in deregulation of small RNAs. *Genetics* **188**: 263–272.

Kurtz S, Phillippy A, Delcher AL, Smoot M, Shumway M, Antonescu C, Salzberg SL. 2004. Versatile and open software for comparing large genomes. *Genome Biology* **5**: R12.

Leal-Bertioli S, Shirasawa K, Abernathy B, Moretzsohn M, Chavarro C, Clevenger J, Ozias-Akins P, Jackson S, Bertioli D. 2015. Tetrasomic recombination is surprisingly frequent in allotetraploid *Arachis*. *Genetics* **199**: 1093–1105.

Levin DA. 2002. The role of chromosomal change in plant evolution. *Systematic Botany* **29**: 460–462.

Levy AA, Feldman M. 2022. Evolution and origin of bread wheat. *Plant Cell* **34**: 2549–2567.

Li LF, Zhang ZB, Wang ZH, Li N, Sha Y, Wang XF, Ding N, Li Y, Zhao J, Wu Y *et al.* 2022. Genome sequences of five Sitopsis species of *Aegilops* and the origin of polyploid wheat B subgenome. *Molecular Plant* **15**: 488–503.

Li Z, McKibben MTW, Finch GS, Blischak PD, Sutherland BL, Barker MS. 2021. Patterns and processes of diploidization in land plants. *Annual Review of Plant Biology* **72**: 387–410.

Lloyd A, Blary A, Charif D, Charpentier C, Tran J, Balzergue S, Delannoy E, Rigaill G, Jenczewski E. 2018. Homoeologous exchanges cause extensive dosage-dependent gene expression changes in an allopolyploid crop. *New Phytologist* **217**: 367–377.

Lloyd A, Bomblies K. 2016. Meiosis in autopolyploid and allopolyploid *Arabidopsis*. *Current Opinion in Plant Biology* **30**: 116–122.

Luo M-C, Gu YQ, Puiu D, Wang H, Twardziok SO, Deal KR, Huo N, Zhu T, Wang L, Wang Y *et al.* 2017. Genome sequence of the progenitor of the wheat D genome *Aegilops tauschii*. *Nature* **551**: 498–502.

Lv R, Wang C, Wang R, Wang X, Zhao J, Wang B, Aslam T, Han F, Liu B. 2022. Chromosomal instability and phenotypic variation in a specific lineage derived from a synthetic allotetraploid wheat. *Frontiers in Plant Science* **13**: 981234.

Mandáková T, Lysak MA. 2018. Post-polyploid diploidization and diversification through dysploid changes. *Current Opinion in Plant Biology* **42**: 55–65.

Mandáková T, Pouch M, Brock JR, Al-Shehbaz IA, Lysak MA. 2019. Origin and evolution of diploid and allopolyploid *Camelina* genomes were accompanied by chromosome shattering. *Plant Cell* **31**: 2596–2612.

Marburger S, Monnahan P, Seear PJ, Martin SH, Koch J, Paajanen P, Bohutínská M, Higgins JD, Schmickl R, Yant L. 2019. Interspecific introgression mediates adaptation to whole genome duplication. *Nature Communications* **10**: 5218.

Marcussen T, Sandve SR, Heier L, Spannagl M, Pfeifer M, Jakobsen KS, Wulff BB, Steuernagel B, Mayer KF, Olsen OA. 2014. Ancient hybridizations among the ancestral genomes of bread wheat. *Science* **345**: 1250092.

Martín AC, Alabdullah AK, Moore G. 2021. A separation-of-function ZIP4 wheat mutant allows crossover between related chromosomes and is meiotically stable. *Scientific Reports* **11**: 21811.

Mason A, Wendel J. 2020. Homoeologous exchanges, segmental allopolyploidy, and polyploid genome evolution. *Frontiers in Genetics* **11**: 1014.

McClintock B. 1984. The significance of responses of the genome to challenge. *Science* **226**: 792–801.

Mercier R, Mézard C, Jenczewski E, Macaisne N, Grelon M. 2015. The molecular biology of meiosis in plants. *Annual Review of Plant Biology* **66**: 297–327.

Mestiri I, Chagué V, Tanguy A-M, Huneau C, Huteau V, Belcram H, Coriton O, Chalhoub B, Jahier J. 2010. Newly synthesized wheat allohexaploids display progenitor-dependent meiotic stability and aneuploidy but structural genomic additivity. *New Phytologist* **186**: 86–101.

Morgan C, Zhang H, Henry CE, Franklin FCH, Bomblies K. 2020. Derived alleles of two axis proteins affect meiotic traits in autotetraploid *Arabidopsis arenosa*. *Proceedings of the National Academy of Sciences, USA* **117**: 8980–8988.

Nicolas SD, Leflon M, Monod H, Eber F, Coriton O, Huteau V, Chèvre A-M, Jenczewski E. 2009. Genetic regulation of meiotic cross-overs between related genomes in *Brassica napus* haploids and hybrids. *Plant Cell* **21**: 373–385.

Nicolas SD, Monod H, Eber F, Chèvre A-M, Jenczewski E. 2012. Non-random distribution of extensive chromosome rearrangements in *Brassica napus* depends on genome organization. *The Plant Journal* **70**: 691–703.

Otto SP. 2007. The evolutionary consequences of polyploidy. *Cell* **131**: 452–462.

Ozkan H, Levy AA, Feldman M. 2001. Allopolyploidy-induced rapid genome evolution in the wheat (*Aegilops–Triticum*) group. *Plant Cell* **13**: 1735–1747.

Ramsey J, Schemske D. 2002. Neopolyploidy in flowering plants. *Annual Review of Ecology and Systematics* **33**: 589–639.

Riley R, Chapman V. 1958. Genetic control of the cytologically diploid behaviour of hexaploid wheat. *Nature* **182**: 713–715.

Ruban AS, Badaeva ED. 2018. Evolution of the S-genomes in *Triticum–Aegilops* alliance: evidences from chromosome analysis. *Frontiers in Plant Science* **9**: 1756.

Schubert I, Lysak MA. 2011. Interpretation of karyotype evolution should consider chromosome structural constraints. *Trends in Genetics* **27**: 207–216.

Sears ER. 1976. Genetic control of chromosome pairing in wheat. *Annual Review of Genetics* **10**: 31–51.

Selmecki AM, Maruvka YE, Richmond PA, Guillet M, Shoresh N, Sorenson AL, De S, Kishony R, Michor F, Dowell R *et al.* 2015. Polyploidy can drive rapid adaptation in yeast. *Nature* **519**: 349–352.

Serra H, Svačina R, Baumann U, Whitford R, Sutton T, Bartoš J, Sourdille P. 2021. *Ph2* encodes the mismatch repair protein MSH7-3D that inhibits wheat homoeologous recombination. *Nature Communications* **12**: 803.

Shaked H, Kashkush K, Ozkan H, Feldman M, Levy AA. 2001. Sequence elimination and cytosine methylation are rapid and reproducible responses of the genome to wide hybridization and allopolyploidy in wheat. *Plant Cell* **13**: 1749–1759.

Shimizu K. 2022. Robustness and the generalist niche of polyploid species: genome shock or gradual evolution? *Current Opinion in Plant Biology* **69**: 102292.

Soltis PS, Marchant DB, Van de Peer Y, Soltis DE. 2015. Polyploidy and genome evolution in plants. *Current Opinion in Genetics & Development* **35**: 119–125.

Soltis PS, Soltis DE. 2009. The role of hybridization in plant speciation. *Annual Review of Plant Biology* **60**: 561–588.

Stebbins GL. 1951. Cataclysmic evolution. *Scientific American* **184**: 54–59.

Stein A, Coriton O, Rousseau-Gueutin M, Samans B, Schiessl SV, Obermeier C, Parkin IAP, Chèvre A-M, Snowdon RJ. 2017. Mapping of homoeologous chromosome exchanges influencing quantitative trait variation in *Brassica napus*. *Plant Biotechnology Journal* **15**: 1478–1489.

Sybenga J. 1996. Chromosome pairing affinity and quadrivalent formation in polyploids: do segmental allopolyploids exist? *Genome* **39**: 1176–1184.

Van de Peer Y, Ashman T-L, Soltis PS, Soltis DE. 2021. Polyploidy: an evolutionary and ecological force in stressful times. *Plant Cell* **33**: 11–26.

Van de Peer Y, Mizrachi E, Marchal K. 2017. The evolutionary significance of polyploidy. *Nature Reviews Genetics* **18**: 411–424.

Veitia RA, Birchler JA. 2022. Gene-dosage issues: a recurrent theme in whole genome duplication events. *Trends in Genetics* **38**: 1–3.

Wang B, Lv R, Zhang Z, Yang C, Xun H, Liu B, Gong L. 2022. Homoeologous exchange enables rapid evolution of tolerance to salinity and hyper-osmotic stresses in a synthetic allotetraploid wheat. *Journal of Experimental Botany* **73**: 7488–7502.

Wang Z, Miao H, Liu J, Xu B, Yao X, Xu C, Zhao S, Fang X, Jia C, Wang J *et al.* 2019. *Musa balbisiana* genome reveals subgenome evolution and functional divergence. *Nature Plants* **5**: 810–821.

Wendel JF. 2000. Genome evolution in polyploids. *Plant Molecular Biology* **42**: 225–249.

Wendel JF. 2015. The wondrous cycles of polyploidy in plants. *American Journal of Botany* **102**: 1753–1756.

Wendel JF, Lisch D, Hu G, Mason AS. 2018. The long and short of doubling down: polyploidy, epigenetics, and the temporal dynamics of genome fractionation. *Current Opinion in Genetics & Development* **49**: 1–7.

Wu Y, Lin F, Zhou Y, Wang J, Sun S, Wang B, Zhang Z, Li G, Lin X, Wang X *et al.* 2021. Genomic mosaicism due to homoeologous exchange generates extensive phenotypic diversity in nascent allopolyploids. *National Science Review* **8**: nwaa277.

Xiong Z, Gaeta RT, Pires JC. 2011. Homoeologous shuffling and chromosome compensation maintain genome balance in resynthesized allopolyploid *Brassica napus*. *Proceedings of the National Academy of Sciences, USA* **108**: 7908–7913.

Zhang H, Bian Y, Gou X, Dong Y, Rustgi S, Zhang B, Xu C, Li N, Qi B, Han F *et al.* 2013a. Intrinsic karyotype stability and gene copy number variations may have laid the foundation for tetraploid wheat formation. *Proceedings of the National Academy of Sciences, USA* **110**: 19466–19471.

Zhang H, Bian Y, Gou X, Zhu B, Xu C, Qi B, Li N, Rustgi S, Zhou H, Han F *et al.* 2013b. Persistent whole-chromosome aneuploidy is generally associated with nascent allohexaploid wheat. *Proceedings of the National Academy of Sciences, USA* **110**: 3447–3452.

Zhang Z, Xun H, Lv R, Gou X, Ma X, Li J, Zhao J, Li N, Gong L, Liu B. 2022. Effects of homoeologous exchange on gene expression and alternative splicing in a newly formed allotetraploid wheat. *The Plant Journal* **111**: 1267–1282.

Zhao N, Zhu B, Li M, Wang L, Xu L, Zhang H, Zheng S, Qi B, Han F, Liu B. 2011. Extensive and heritable epigenetic remodeling and genetic stability accompany allohexaploidization of wheat. *Genetics* **188**: 499–510.

Zhu J, Tsai H-J, Gordon MR, Li R. 2018. Cellular stress associated with aneuploidy. *Developmental Cell* **44**: 420–431.

Supporting Information

Additional Supporting Information may be found online in the Supporting Information section at the end of the article.

Fig. S1 Synthesis of the allotetraploid wheat (S^bS^bDD), its cytological validation, its spike morphology relative to parental species, and construction of the 'genetic variant-accumulating population' (population I).

Fig. S2 Diagrammatic illustration of construction of the 'multigenerational euploidy-selecting population' (population II) of the synthetic allotetraploid wheat (S^bS^bDD).

Fig. S3 Diagram of proportion of syntenic sequence calculation.

Fig. S4 Differences in frequencies of numerical chromosomal variations and structural chromosomal variations among chromosomes and between the two subgenomes in the 'multigenerational euploidy-selecting population' (population II) of the synthetic allotetraploid wheat (S^bS^bDD).

Fig. S5 Correlations of the various relevant homoeologous chromosome pairing irregularities at MI (quandrivalents, trivalents, and hetero-bivalents) with structural chromosomal variations.

Fig. S6 Structural variants detected by synteny and rearrangement identifier between the genomes of *Aegilops bicornis* (reference) and *Aegilops tauschii* (query).

Fig. S7 Correlations of homoeologous chromosome pairing irregularities at MI with each of the genomic features reflecting genetic affinity between the two parental genomes.

Fig. S8 Delineation of the centromere regions of chromosomes 2–7 (chromosome 1 was shown in Fig. 8) based on the distribution densities of genes and transposable elements.

Fig. S9 Correlations between sequence synteny at each of the 21 divided chromosomal regions at equal length (in nt) and homoeologous chromosome pairing irregularity at MI of pollen mother cells.

Fig. S10 Correlations between sequence synteny at each of the 31 divided chromosomal regions at equal length (in nt) and homoeologous chromosome pairing irregularity at MI of pollen mother cells.

Fig. S11 Correlations between sequence synteny at each of the 41 divided chromosomal regions at equal length (in nt) and homoeologous chromosome pairing irregularity at MI of pollen mother cells.

Fig. S12 Correlations of homoeologous chromosome pairing irregularities at MI with each of the variables reflecting genomic features besides genic synteny at each of the 41 divided chromosomal regions at equal length (in nt) between the two parental genomes.

Fig. S13 Correlations between sequence synteny at each of the 41 divided chromosomal regions at equal length (in nt) and each type of homoeologous chromosome pairing irregularity at MI of pollen mother cells, that is, quadrivalents, trivalents, and hetero-bivalents, separately.

Methods S1 Mitotic and meiotic karyotyping by florescence *in situ* hybridization and genomic *in situ* hybridization.

Notes S1 Numerical and structural chromosomal variation in the 'euploidy-selectin population' (population II).

Table S1 List of detailed mitotic karyotypes of a 1322 individual plants in the S8 generation of the synthetic allotetraploid wheat (S^bS^bDD).

Table S2 List of detailed meiotic karyotypes at MI of a total of 360 pollen mother cells from 10 analyzed euploid plants.

Table S3 Cook's distance of the seven sets of homoeologous chromosome pairs for quadrivalent, trivalent, and hetero-bivalent.

Table S4 Chromosome length, overall synteny, genic synteny, genic nucleotide similarity, structural variants, and content of transposable elements of the seven set of homoeologous chromosome pairs of *Aegilops bicornis* and *Aegilops tauschii*.

Table S5 Number, length, and proportion of syntenic sequences in the 21, 31, and 41 equal length (in nt) chromosomal regions of the seven sets of homoeologous chromosome pairs of *Aegilops bicornis* and *Aegilops tauschii*.

Please note: Wiley is not responsible for the content or functionality of any Supporting Information supplied by the authors. Any queries (other than missing material) should be directed to the *New Phytologist* Central Office.